(p, pα) And (α, 2α) Reactions at Medium-Energy and Alpha-clustering Correlations in Light Nuclei

AUTHOR(S):

Takimoto, Kiyohiko

Memoirs of the College of Science, University of Kyoto, Series A,
Vol. XXXI, No. 2, Article 12, 1967.

$(p, p\alpha)$ AND $(\alpha, 2\alpha)$ REACTIONS AT MEDIUM-ENERGY AND ALPHA-CLUSTERING CORRELATIONS IN LIGHT NUCLEI

BY

Kiyohiko TAKIMOTO

Department of Physics, Faculty of Science, Kyoto University, Kyoto, Japan

SYNOPSIS

The energy correlation and angular correlation distributions between two emitted particles from the $(\alpha, 2\alpha)$ and $(p, p\alpha)$ reactions on some light nuclei were obtained and the reaction mechanism and the alpha-clustering correlation were investigated. The reactions studied were: the $(\alpha, 2\alpha)$ reactions on Be^9 at 28.0, 32.3 and 37.4 MeV, B^{10} at 28.4 MeV, C^{12} at 28.0 and 37.4 MeV and O^{16} at 26.5 MeV, and the Be^9 $(p, p\alpha)$ He^5 reaction at 55 MeV.

Peaks corresponding to the low lying states of the residual nuclei were found in the summed energy spectra, and the angular correlation distributions were obtained for the two emitted particles leading to the ground state of the residual nucleus. The energy correlation and the angular correlation distributions between the symmetrically emitted two particles were explained by assuming a quasi-free scattering process with the plane wave impulse approximation. The amplitudes and the shapes of the intranuclear momentum distribution of the alpha-cluster show that the alpha-clustering correlation is strong in Be^9, fairly strong in B^{10}, weak in C^{12} and rather strong in O^{16}.

1. Introduction

The concept of cluster structure provides a new tool for the further understanding of nuclear structure. In the surface of heavier nuclei and in the whole body of light nuclei, many phenomena related to many nucleon correlation have been observed and discussed. In heavier nuclei the nuclear density distribution quickly falls off at the surface region, and in light nuclei the constant nuclear density region scarcely exists and the surface region spreads throughout the nucleus.[1] In these diffuse density region, there exist many unoccupied states in the Fermi sea, so that the many particle correlation can easily take place. This correlation can scarcely exist in the infinite nuclear matter, because the states are completely occupied[2] and the two-body correlation is essential in this case. Because the number of nucleons in the nucleus is finite, the character of the nuclear surface region has an important effect upon the whole nuclear properties. Then the cluster structure in the surface region plays an important role upon the properties of nuclei.[2] Moreover, to get deep insight of the properties of nuclear structure on the bases of the realistic two-body nuclear forces, knowledge on the many nucleon correlations is necessary and useful.

The structure of light nuclei has been discussed within the framework of

cluster models by several authors. One of them treats nucleon clusters as constructed by the correlation between the nucleons in Hartree-Fock potential,[3] and the others use the resonating group methods.[4,5] In Ref. 5), the interaction between the clusters was derived from realistic two-body nuclear force. Such a treatment may be one of the useful methods to understand the nuclear structre on the bases of the realistic two-body nuclear force.

The experimental investigation about the cluster structure has been performed concerning the following phenomena; cluster transfer reaction,[6] quasi-free cluster knock-out reaction,[7] high energy spallation reaction,[8] absorption of gamma quanta, π^- meson and K^- meson by quasi-α particles,[9] and the quasi-molecular states in heavy ion collisions[10]. These phenomena provide important information on the nucleon cluster structure. Among them, the cluster stripping or pick-up reaction and the quasi-free knock-out reaction can give more precise information than others. In particular, the latter reaction is the most useful, because the reaction mechanism can be uniquely assigned and the form factor of the relative wave functions between a cluster and the residual part in the nucleus can be decided in this reaction.

Among possible types of nucleon cluster in the nucleus, the alpha cluster is the most interesting in the first place. The binding energy of an alpha-particle is large compared with that of He^3, T, D etc., while the interaction between two alpha-particles is rather weak. These facts result from the characteristics of the two-body nuclear force, the charactor of strong tensor force and of charge symmetry.[11] Then it is very interesting and valuable to study how the alpha-clustering is maintained in the nuclear many-body system, and how the alpha-clustering affects the nuclear properties.

Up to now, experiments on the quasi-free knock-out reaction have been done using relatively high energy incident particles. But if medium energy particles are used, some of the difficulties appeared in the high energy experiment are removed. The first merit is that the individual states of the final nucleus can be separated because of the better energy resolution in the absolute value. Actually, in the experiments of high energy $(p, p\alpha)$[12] and $(\alpha, 2\alpha)$[13] reactions hitherto made, the individual states of the final nucleus have not been resolved. The second merit comes from the relatively large yields of the quasi-free scattering. For example, the differential cross section of $\alpha-\alpha$ scattering at 90° in the center-of-mass system is about 0.5 (mb/st.) at 120 MeV incident energy, while, at 53.4 MeV, that is about 100 (mb/st.),[14] so the yield of the quasi-free alpha-alpha scattering can be expected to increases at low energy. In general, as the yield of the quasi-free scattering are not so large, the relatively large yield markedly benefits the accuracy of the experiment. Still more, when high energy particles collide with the nucleon cluster in the nucleus, the clustering correlations are easily broken, and the observation of the emitted particles cannot completely inform us the clustering correlations in the nucleus.

It is appropriate to call a $(x, x\alpha)$ reaction a quasi-free $x-\alpha$ scattering, if this reaction somewhat resembles a free $x-\alpha$ scattering. This scattering means that the reaction can be approximately considered as a collision between two classical particles, the projectile and the bound alpha-particles. This condition is satisfied when the energy of the incident particle is so high that the de Broglie wavelength is sufficiently small to identify an alpha-particle in the target nucleus. In this

case, the reaction mainly occurs due to the direct interaction between the incident and the knocked-out particle, and the reaction cross section may be expressed in terms of the free $x-\alpha$ scattering cross section at the relevant energy and scattering angle. In this way one can circumvent the lack of precise knowledge of the $x-\alpha$ interaction in the nucleus and can extract the information directly related to the motion of the alpha-cluster in the nucleus.

Actually, the direct interaction model of the reaction mechanism as sketched above predicts that the momentum distribution of the recoiled residual nucleus (we call it the recoil momentum distribution hereafter), is equal to that of the alpha-particle bound in the target nucleus, if the interaction between the residual nucleus and the incoming particle and the interaction between the residual nucleus and the outgoing particle are neglected. This prediction follows from the natural assumption that the residual nucleus (or core as one can call it when it is a part of the target nucleus) will continue to move as it did before the impact of the incoming particle if the alpha-particle is removed in a very short time interval compared with the period of the relative motion between the alpha-particle and the core. Before impact, the bound alpha-particle and the core must always move with exactly equal and opposite momenta since the target as a whole is at rest. The existence of interactions between the core and the incoming or outgoing alpha-particles will modify this assumption of the process, and this modification is more serious in the medium energy reaction.

Quasi-free knock-out $(x, x\alpha)$ reation is restricted by the kinematical conditions similar to those of a corresponding free scattering process. Using the laws of conservation of energy and momentum the follwing equation are given

$$E_0=E_x+E_\alpha+E_R+E_s \qquad \cdots\cdots\cdots\cdots(1)$$

$$\boldsymbol{k}_0=\boldsymbol{k}_x+\boldsymbol{k}_\alpha+\boldsymbol{k}_R \qquad \cdots\cdots\cdots\cdots(2)$$

where E_0, E_x and E_α are the energies of the incident particles and the two outgoing particles respectively, and $\hbar\boldsymbol{k}_0$, $\hbar\boldsymbol{k}_x$ and $\hbar\boldsymbol{k}_\alpha$ mean the momenta of them respectively. The tsubscript x is used to the incident and outgoing proton or alpha-particles and α means the struck-out alpha-particle. E_s is the separation energy of the alpha-particle, i. e. the energy necessary to separate the bound alpha particle from the target leaving the residual nucleus in a definite final state. Representing the excitation energy of the residual nuleus by E_{ex}, the separation energy is equal to the algebraic sum of the reaction Q-value and E_{ex}, i. e. $E_s=E_{ex}-Q$. E_R is the kinetic energy of the residual nucleus and is related to the recoil momentum $\hbar\boldsymbol{k}_R$ by

$$E_R=\frac{\hbar^2\boldsymbol{k}_R^2}{2M_R} \qquad \cdots\cdots\cdots\cdots(3)$$

with M_R being the mass of the residual nucleus.

In the quasi-free scattering experiment, coincidence techniques are usually employed to decide the E_x, E_α, $\hbar\boldsymbol{k}_x$ and $\hbar\boldsymbol{k}_\alpha$ simultaneously. The incident energy E_0 and the incident momentum $\hbar\boldsymbol{k}_0$ are known. Now the reaction cross section can be expressed as a function of summed-energy $E_x+E_\alpha+E_R(=E_0-E_s)$. For a given value of $E_x+E_\alpha+E_R$ the cross section is a function of $\hbar\boldsymbol{k}_R$. We call the former function "summed energy spectrum" and the latter "recoil momentum distribution". The recoil momentum $\hbar\boldsymbol{k}_R$ equals the momentum $-\hbar\boldsymbol{k}$ of the alpha-cluster, so, from these measured values the information on the motion of the alpha-

cluster in the target nucleus is given. The summed-energy spectrum gives directly the separation energy of an alpha particle in the target nucleus which leaves the residual nucleus in some excited state.

The analysis is much simplified when the experiment is performed in a symmetric and coplanar geometry, i. e. in a way that the outgoing particles with momenta which are coplanar with the beam and symmetric each other to the beam are selected. Then, the following expression for $\hbar k_R$ the component of the recoil momentum along the incident beam, is given

$$k_R = k_0 - 2k_\alpha \cos\theta \qquad \cdots\cdots(4)$$

where, because of the symmetry,

$$k = |\boldsymbol{k}_x| = |\boldsymbol{k}_\alpha|,\ \theta_x = \theta_\alpha = \theta,\ k_R = |\boldsymbol{k}_R| \qquad \cdots\cdots(5)$$

Even when $|\boldsymbol{k}_R| = 0$, i. e., when alpha-particles are at rest in the nucleus, the angle θ is somewhat smaller than that expected from the free scattering due to the separation energy.

In the present work, the properties of the alpha-clustering correlations in Be^9, B^{10}, C^{12} and O^{16} nuclei are studied with the $(\alpha, 2\alpha)$ and the $(p, p\alpha)$ reactions on these nuclei.* The Be^9 $(\alpha, 2\alpha)$ He^5 reaction was observed at the incident alpha-particle energy of 28.0,[15] 32.3 and 37.4 MeV.[16] Also, the Be^9 $(p, p\alpha)$ He^5 reaction[17] was observed at the incident proton energy of 55 MeV. The B^{10} $(\alpha, 2\alpha)$ Li^6 reaction[18] was investigated at the incident alpha-particle energy of 28.4 MeV. The C^{12} $(\alpha, 2\alpha)$ Be^8 [16] reactions was performed at 28.0[15,19] and 37.4 MeV alpha energy. Finally the O^{16} $(\alpha, 2\alpha)$ C^{12} [19] reactions was observed at 26.5 MeV alpha-particle energy. In each reaction, as described above, the energy correlation distributions and the angular correlation distributions between the emitted particles were obtained.

In this paper, the experimental results of these reactions are presented. The experimental results are analysed by assuming the quasi-free scattering process. Some informations on the alpha clustering correlations in these light nuclei are discussed.

2. The Experimental Procedures

2.1. $(\alpha, 2\alpha)$ Reactions

2.1.1. *General*

In the experiments at Kyoto University, alpha particles of about 28 MeV from a 105 cm cyclotron were used. The beam spread at the center of the scattering chamber was about 3.5 mm in diameter. The beam current was integrated electronically and used as a beam monitor. In the experiments at the Institute for Nuclear Study, University of Tokyo, alpha particles of 32.3 MeV and 37.4 MeV from an energy variable cyclotron were used. The beam spread at the center of the scattering chamber was about 3.5 mm in diameter. The beam current was integrated electronically and used as a beam monitor. The yield of the elastically scattered alpha particles from the target at one angle was used as a target monitor simultaneously.

The schematic diagram of the experimental arrangement is shown in Fig. 1.

* The author is much indebted to the authors of Ref. 16)~19), for allowing him to use the experimental data before publication.

Two detectors were mounted on two movable arms respectively, and could be rotated independently in the same plane containing the beam axis. Silicon semiconductor detectors of $p-n$ junction type and also of surface-barrier type were used as alpha particle detectors. The depletion layers of the both types of the detectors were thick enough to stop 30 MeV alpha-particles. They were placed just behind the defining apertures of 3 or 4 mm in diameter which were about 10 cm apart from the target center.

A block diagram of the electronic system used in the experiments is shown in Fig. 2. Pulses from the detectors were amplified with the voltage sensitive preamplifiers and the fast amplifiers. The rise time and the full width of the output

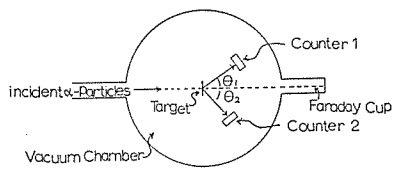

Fig. 1. A schematic diagram of the experimental arrangement for the measurement of the $(\alpha, 2\alpha)$ reactions.

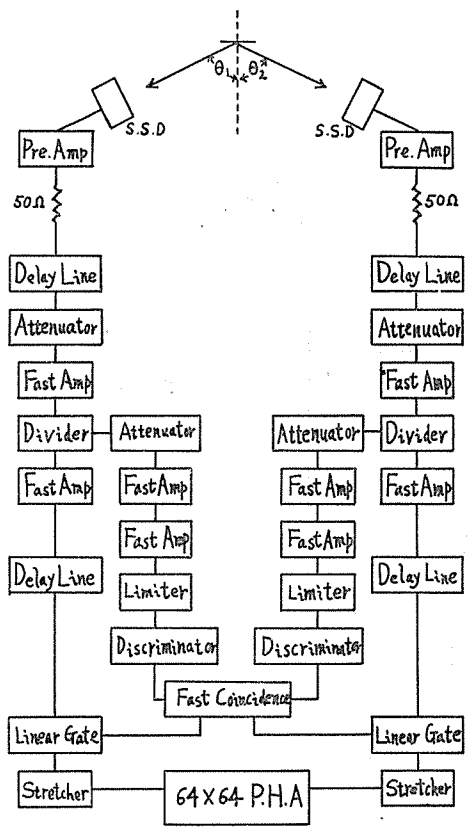

Fig. 2. A block diagram of the electronic system for the measurement of the $(\alpha, 2\alpha)$ reactions.

pulses were about 15 ns and less than 50 ns respectively. Then the pulses were divided into two parts; the one was used as a timing signal and the other as an energy signal. The timing pulses were discriminated and shaped to the 20 ns width rectangular pulses and then fed into a fast coincidence circuit with $2\tau = 4 \times 10^{-8}$ sec resolving time. The energy signals were fed into a pulse-height-analyser, only when the gate were opened by the output pulse of the coincidence circuit. Signals from each detector were fed into the input connectors of a two-dimensional pulse-height-analyser; 32×32 channel or 64×64 channel P. H. A.. The resolving time of the coincidence circuit was sufficiently shorter than the time interval of the beam bunches of the cyclotron, that were 7.7×10^{-8} sec for Kyoto University cyclotron and 1.13×10^{-7} sec, and 1.05×10^{-7} sec, for INS cyclotron corresponding to 28, 32.3 and 37.4 MeV alpha-particle beams, respectively. With this condition the two-dimensional pulse-height-analyser registers only the events arose in the period of one beam bunch.

The random coincidence counts were estimated by delaying the timing of one of the two detectors by the time interval of the beam bunches. The random coincidence runs were carried out whenever the true coincidence runs were done and the random coincidence rates were less than a few percent of the true coincidence rates at most angles. Only at the extreme forward angles the rates were about ten percent. The stability of the electronic system was checked by measuring the peak of alpha-particles elastically scattered by the target, before and after each true or random coincidence runs.

The timing adjustment and the energy calibration of the whole counting system were set by using alpha-alpha scattering and the elastic scattering of alpha-particles by the target nuclei.

The angular resolution of the counter system for the coincidence measurement was checked by detecting the angular correlation distribution between the elastically

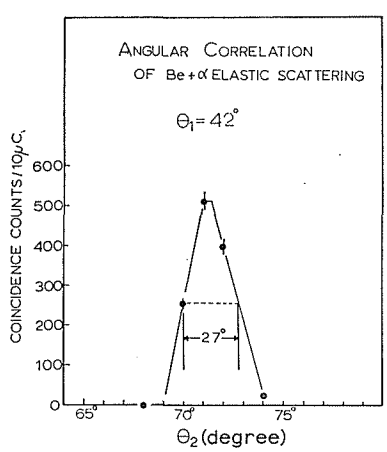

Fig. 3. An angular correlation distribution between the elastically scattered alpha-particle and the recoiled Be^9 nucleus.

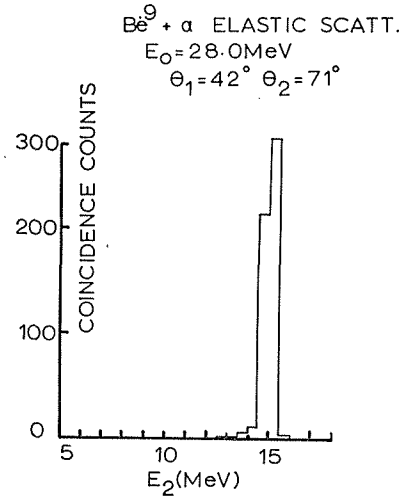

Fig. 4. A single energy spectrum of the elastically scattered alpha-particle from the Be^9 nucleus when the coincidence measurement was performed.

scattered alpha-particle and the recoiled target nucleus. The experimental angular resolution was scarcely different from the values calculated from the geometrical condition. An example of such measurement is given in Fig. 3. for the $Be^9-\alpha$ system. The energy resolutions of the detector system for the angular correlation measurement were also checked by using the same phenomenon. One of the results is given in Fig. 4. In this case the energy resolution of a single counter was about 1 MeV in full width. In most cases better resolutions were attained. Only in the case of O^{16}, the energy resolution was worse ($\sim$2 MeV.) because the oxygen gas target was used.

Two dimensional pulse height distributions were measured at each pair of θ_1 and θ_2 between the coincident two alpha-particles (the notation given in Fig. 1. is used hereafter). The differential cross sections can be determined as functions of four parameter, (θ_1, E_1, θ_2, E_2). These four parameters completely decide the kinematics of the three body system in a coplane. Two different methods to measure the angular correlation distribution were adopted; the one has a symmetric geometry described in Section 1., and the other has non-symmetric geometry where θ_1 is fixed at a certain value and θ_2 is varied. In the former method the recoil momentum $\hbar\boldsymbol{k}_R$ relates directly to the angle θ ($=\theta_1=\theta_2$). In the latter method the recoil momentum which lies in other direction than that of the beam is observable and further the mixing of the sequential two-body decay process can be checked. This sequential process means that at first an incident alpha-particle is inelastically scattered by the target nucleus and then the recoiled nucleus in an excited state emits an alpha-particle.

In order to distinguish this process from the direct knock-out process with the aid of kinematical consideration, the variation of the energy spectrum of fixed counter accompanied with the change of θ_2 must be measured. Examples of the relation of $|\boldsymbol{k}_R|$ vs. (E_1, θ_1, E_2, θ_2) are given in Fig. 5. (symmetric geometry)

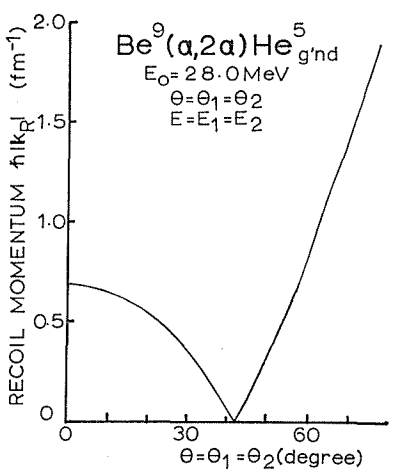

Fig. 5. A kinematical relation of $|\boldsymbol{k}_R|$ vs. (E_1, θ_1, E_2, θ_2,) for the Be^9 (α, 2α) He^5g'nd ($Q\simeq-2.5$ MeV) reaction at 28.0 MeV in the symmetric geometry ($\theta=\theta_1=\theta_2$, $k=|\boldsymbol{k}_1|=|\boldsymbol{k}_2|$).

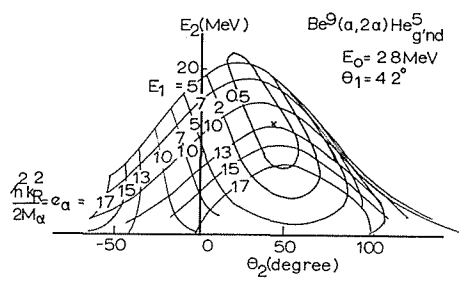

Fig. 6. A kinematical relation of $|\boldsymbol{k}_R|$ vs. (E_1, θ_1, E_2, θ_2) for the Be^9 (α, 2α) He^5g'nd ($Q\simeq-2.5$ MeV) reaction at 28.0 MeV in a non-symmetric geometry (θ_1 is fixed at 42° and θ_2 is varied.)

and in Fig. 6. (non-symmetric geometry), for the Be^9 $(\alpha, 2\alpha)$ $He^5_{g'nd}$ reaction at 28.0 MeV.

The average beam current was about 0.05 μA throughout the experiments. The amount of alpha-particle beam used in each run was about 100 μ Coulomb.

2. 1. 2. Be^9 $(\alpha, 2\alpha)$ He^5 *Reaction*

The experiments were performed using 28.0, 32.3 and 37.4 MeV alpha-particles. The target of Be^9 was a self-supported thin foil prepared by vacuum evaporation and the thickness of the foil used was ranged from 0.11 mg/cm^2 to 0.83 mg/cm^2. The solid angle subtended by each counter was about 1×10^{-3} steradian in all cases.

In the experiment at 28.0 MeV, four kinds of the angular correlation distribution were measured. They were: (i) $\theta=\theta_1=\theta_2$, $\theta=22°-70°$. (ii) $\theta_1=30°$, $\theta_2=20°-70°$, (iii) $\theta_1=35°$, $\theta_2=20°-70°$, (iv) $\theta_1=42°$, $\theta_2=22°-82°$.

In the experiments at 32.3 MeV and 37.4 MeV, only the symmetric method was adopted ($\theta=15°-60°$ in the former and $\theta=15°-70°$ in the latter).

2. 1. 3. B^{10} $(\alpha, 2\alpha)$ Li^6 *Reaction*

The experiment was performed using 28.4 MeV alpha-particles. The target of B^{10} was a self-supported thin foil prepared by vacuum evaporation of 99% enriched B^{10} isotope and the thickness of the foils used during the experiments was 0.16 mg/cm^2.

Two kinds of the angular correlation distribution were measured: (i) ($\theta=\theta_1=\theta_2$, $\theta=16°-70°$) (ii) ($\theta_1=40°$, $\theta_2=15°-75°$).

2. 1. 4. C^{12} $(\alpha, 2\alpha)$ Be^8 *Reaction*

The experiment was performed using 28.0 MeV and 37.4 MeV alpha-particles. The target of C^{12} was a self-supported thin foil prepared by vacuum evaporation or by thermal cracking of CH_4 gas. The thickness of the foil used was ranged from 0.1 mg/cm^2 to 1 mg/cm^2.

In the experiment at 28.0 MeV, four types of the angular correlation distribution were measured: (i) $\theta=\theta_1=\theta_2$, $\theta=25°-60°$ (ii) $\theta_1=25°$, $\theta_2=20°-65°$, (iii) $\theta_1=35°$, $\theta_2=20°-70°$, (iv) $\theta_1=50°$, $\theta_2=20°-70°$.

In the experiment at 37.4 MeV, only the symmetric method was adopted ($\theta=\theta_1=\theta_2$, $\theta=12.5°-67.5°$).

2. 1. 5. O^{16} $(\alpha, 2\alpha)$ C^{12} *Reaction*

The experiment was performed by using 28.0 MeV alpha-particles. The target of O^{16} was natural oxygen gas of 99.9% purity at the pressure of 40 cm Hg. The energy of the incident alpha-particles was 26.5 MeV at the center of the gas target. The angular resolution in this gas target system was measured by $\alpha-He^4$ scattering and was about 6°. The energy resolution was measured to be ~2.0 MeV.

The angular correlation distribution was measured only by the symmetric method ($\theta=\theta_1=\theta_2$, $\theta=20°-65°$).

2. 2. Be^9 $(p, p\alpha)$ He^2 Reaction

Protons of about 55 MeV was obtained from a synchlo-cyclotron of the Institute for Nuclear Study, University of Tokyo. The beam spread at the center of the scattering chamber was about 10 mm in height and in width. The beam current was integrated electronically and used as a beam monitor.

The schematic diagram of the exprimental arrangement is shown in Fig. 7. A proton counter and an alpha-particle counter were mounted on the two moving arms respectively, and could be rotated independently in the same plane containing

the beam axis. The proton counter was composed of an lead absorber and two silicon semiconductor detectors. The lead absorber was placed so that the protons of less than 26.0 MeV were stopped. The front detector was a lithium-drift silicon transmission detector whose depletion layer was 3 mm in thickness. The rear detector was a lithium-drift S. S. D. whose depletion layer was 5 mm in thickness. These two detectors were coupled as a telescope. As a whole, the proton counter selects out the protons having kinetic energy more than 35.5 MeV. The proton counter was placed just behind the defining apperture of 4 mm in diameter which was about 9.85 cm apart from the target center. The alpha counter was composed of three surface-barrier silicon detectors. The thickness of their depletion layer was 100 microns, 500 microns and 2 mm respectively. By the front detector (100 μ), the low-energy alpha-particles (less than 12 MeV) were detected and the signals of the penetrated particles were gated-off by the signals from the middle detector.

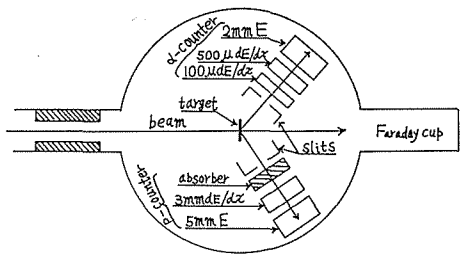

Fig. 7. A schematic diagram of the experimental arrangement for the measurement of the Be^9 (p, $p\alpha$) He^5 reaction.

The front detector also detected only the protons of less than 3 MeV and the deuterons of less than 4 MeV. The middle detector (500 μ) was used to detect the alpha-particles of more than 12 MeV and less than 35 MeV, by the same method as above. The middle detector also detected only protons of the energy from 3 MeV to 9 MeV and deuterons of the energy from 4 MeV to 12 MeV. The alpha counter was placed just behind the defining aperture of 4 mm in diameter which was about 9.95 cm apart from the target center.

A block diagram of the electronic system is shown in Fig. 8. Pulses from each detectors were amplified with a fast pre-amplifier. The output signals had the rise time of about 15 ns and the width about 50 ns for 100 μ and 500 μ S. S. D. and the rise time of about 30~40 ns and the width of about 100 ns for 2 mm, 3 mm and 5 mm S. S. D. Pulses from the two detectors of the proton counter were fed into a fast coincidence circuit (its resolving time

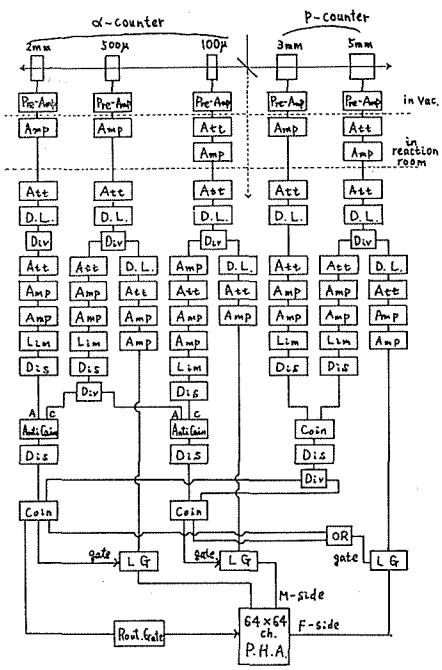

Fig. 8. A block diagram of the electronic system for the measurement of the Be^9 (p, $p\alpha$) He^5 reaction.

was $2\tau=40$ ns.). Although pulses from the detector had a relatively long rise time, the time ripple of the coincidence was less than 10 ns because the pulses were amplified sufficiently so as to trigger the fast discriminator much before the full rise. The coincident output was fed into the next coincidence circuits. For the alpha counter, output signal from the $100\mu-500\mu$ anti-coincidence circuit, was fed into the next coincidence circuit. This coincidence circuit selected the pulses from the proton counter and the alpha counter and its output signal opened the gates of the energy pulses from the $100\,\mu$ and the 5 mm detectors. The resolving time of the whole coincidence system was $2\tau=6\times10^{-8}$ sec. Within this time interval two bunches of the proton beam could be included. The proton spectrum was registered in the one side (64 ch) of the two-dimensional pulse-height-analyser (ND 4096) and the alpha-particle spectrum in the other side, which was divided into two parts (2×32 ch) and the low-energy alpha-particles and the high-energy alpha-particles were separately fed into each part with the use of ROUTE GATE.

The random coincidence counts were estimated by delaying the timing of one of the two counters by two time intervals of the beam bunches. The random coincidence runs were carried out every after the true coincidence runs and the random coincidence rate was less than a few percent of the true coincidence rate at most angles except at an extremely forward angle. This good signal-to-noise ratio was attributed to the telescope system of the proton counter and the anti-coincidence system of the alpha counter.

The target of Be^9 was a self-supported thin foil prepared by vacuum evaporation and the thickness of the foil was 1.4 mg/cm^2 and the size was 15 mm in diameter.

The timing adjustment and the energy calibration of the whole counting system were set by coincidence measurement of the proton-proton scattering using a polyethylene film as a target and the proton-Be^9 elastic scattering. For the proton and alpha-particle system the timing was modified according to the difference of the flight time.

The angular correlation distribution was measured only by the symmetric method. The relation among the recoil momentum $\hbar|\boldsymbol{k}_R|$, the symmetrical angle θ $(=\theta_p=\theta_\alpha)$ and the momentum of the emitted particle $\hbar|\boldsymbol{k}_p|$ $(=\hbar|\boldsymbol{k}_\alpha|)$ for the Be^9 $(p, p\alpha)$ He^5 reaction was calculated according to the eqs. (1)$\sim$(5) and is shown in Fig. 9.

The average beam current was $0.04\,\mu$A of the debunched beam. The amount of proton beam for each run was about $50\,\mu$ Coulomb, and at the recoilless angle ($\theta=55°$) four runs were accumulated. At each angle, a random coincidence run was carried

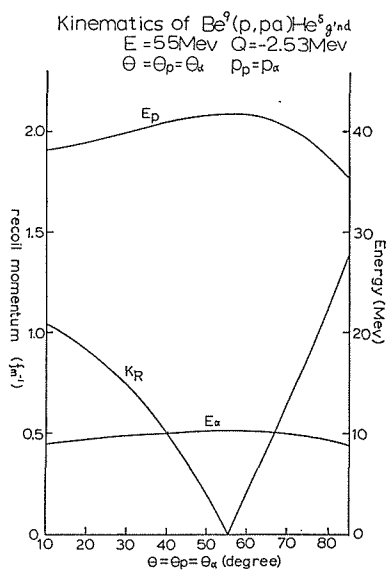

Fig. 9. A kinematical relation among the recoil momentum $\hbar|\boldsymbol{k}_R|$, the symmetrical angle $\theta(=\theta_p=\theta_\alpha)$ and the momentum of the emitted particle $\hbar|\boldsymbol{k}_p|$ $(=\hbar|\boldsymbol{k}_\alpha|)$ for the Be^9 $(p, p\alpha)$ $He^5g'nd$ $(Q\simeq-2.5$ MeV) reaction $(\theta_p=\theta_\alpha,\ \hbar|\boldsymbol{k}_p|=\hbar|\boldsymbol{k}_\alpha|)$ at 55 MeV. For the notations see in text.

out using about a half of amount of proton beam for a true coincidence run. As a monitor, a surface-barrier silicon detector with the depletion layer of 1.5 mm in thickness was set behind the 1.5 mm aluminium absorber at 45° and the elastically scattered protons by the target were detected.

3. Experimental Results

3.1. Be^9 (α, 2α) He^5 Reaction

The summed energy spectra are given in Fig. 10. The abscissa shows the summed energy ($E_1+E_2+E_R$) and the excitation energy of the residual He^5 nucleus. The set of $\theta_1-\theta_2$ cited in the figure is the recoilless angle, when the He^5 nucleus is left in the ground state. There exists a sharp peak at the summed-energy corresponding to the ground state of He^5 nucleus ($Q\simeq-2.5$ MeV) in each case. About this peak the data are decomposed to give the angular correlation distributions at the three energies. At 32.3 MeV and 37.4 MeV, about the region around $Q\simeq-7.0$ MeV (corresponding to the 1st excited state of He^5 nucleus) the angular correlation distributions are also obtained. Furthermore, at 37.4 MeV about the region around $Q\simeq-19.2$ MeV (corresponding to the 2nd excited state of He^5 nucleus) the angular correlation distribution is obtained.

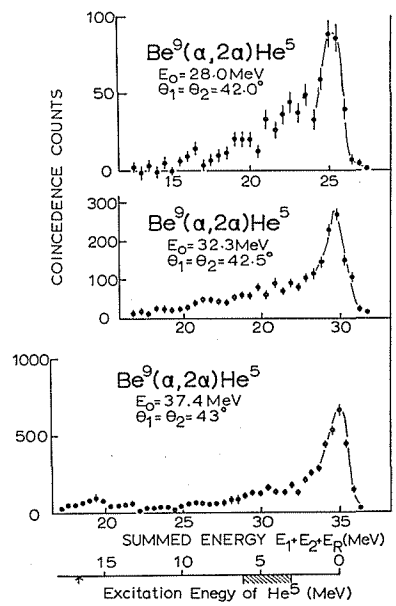

Fig. 10. The summed-energy spectra of the emitted alpha-particles from the Be^9 (α, 2α) He^5 reactions at 28.0, 32.3 and 37.4 MeV respectively, when both counters are set at the recoilless angles for the Q-value of -2.5 MeV in the symmetric method. The abscissa shows the summed energy ($E_1+E_2+E_R$) and the excitation energy of the residual He^5 nucleus.

Figs. 11~14. show four kinds of the angular correlation distribution for the Be^9 (α, 2α) $He^5{}_{g'nd}$ reaction at 28.0 MeV. The distributions is shown for each 2.5 MeV interval of E_1, and in each interval the four kinematical parameters are determined within the experimental resolution. When E_1 is 11.5

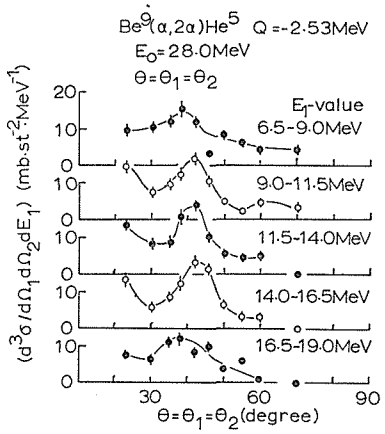

Fig. 11. The angular correlation distributions for the Be^9 (α, 2α) $He^5{}_{g'nd}$ ($Q\simeq-2.5$ MeV) reaction at 28.0 MeV obtained by the symmeric method ($\theta_1=\theta_2$). The distribution is shown for each 2.5 MeV interval of E_1.

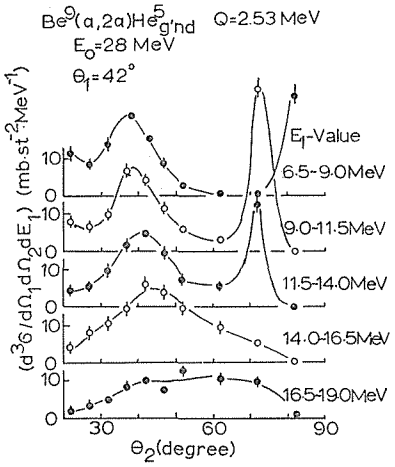

Fig. 12. The angular correlation distributions for the Be^9 $(\alpha, 2\alpha)$ $He^5_{g'nd}$ ($Q\simeq -2.5$ MeV) reaction at 28.0 MeV obtained by the non-symmetric method when θ_1 is fixed at 42°. The distribution is shown for each 2.5 MeV interval of E_1.

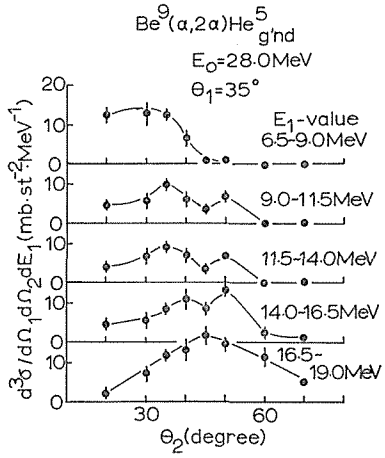

Fig. 13. The angular correlation distributions for the Be^9 $(\alpha, 2\alpha)$ $He^5_{g'nd}$ ($Q\simeq -2.5$ MeV) reaction at 28.0 MeV obtained by the non-symmetric method when θ_1 is fixed at 35°. The distribution is shown for each 2.5 MeV interval of E_1.

MeV−14.0 MeV, the condition $E_1\simeq E_2$ is held.

Fig. 11 gives the results obtained by the symmetric method. Among these distribution curves that of $E_1\simeq E_2$ can be directly compared with Fq. (5) and Eq. (6).

Fig. 12 gives the results obtained by the non-symmetric method when θ_1 is fixed at 42°. As seen in Figs. 11 and 12, the differential cross sections have a maximum value about the recoilless angle ($=42°=\theta_1=\theta_2$, if $E_1=E_2$). This fact proves that the quasi-free alpha-alpha scattering process is realised. In Fig. 12, there exists another sharp peak at backward angles for some energy intervals, but this is tailings due to coincident pulses of elastically scattered alpha-particles and recoil Be^9 nuclei. These surplus coincidence events can be selected out if the energy loss of Be ions is little before arrival at the active layer of the detector.

Figs. 13 and 14 give the results obtained by the non-symmetric method when θ_1 is fixed at 35° and at 30° respectively. In Figs. 13 and 14, the recoilless point is not existent if $E_1\simeq E_2$, but exists in larger E_1 and θ_2. If $\theta_1=35°$, the recoilless point exists at $E_1=16.0$ MeV and $\theta_2=50°$, and if $\theta_1=30°$, at $E_1=18.5$ MeV and $\theta_2=55°$. In both cases the maxima of the differential cross section are observed in these points.

Figs. 15 and 16 show the angular correlation distributions of the alpha-particles obtained by the symmetric method at 32.3 MeV. In Fig. 15, the angular correlation distributions about the region of $Q\simeq -2.5$ MeV are shown for each 2.5 MeV interval of E_1. If $E_1\simeq E_2$, the recoilless angle is 42.5° and a maximum of the differential cross section occurs at this angle, as is observed at 28 MeV. In Fig. 16, the angular correlation distributions about the region around $Q\simeq -7.0$ MeV are shown.

Figs. 17∼19 show the angular correlation distributions of the alpha-particles

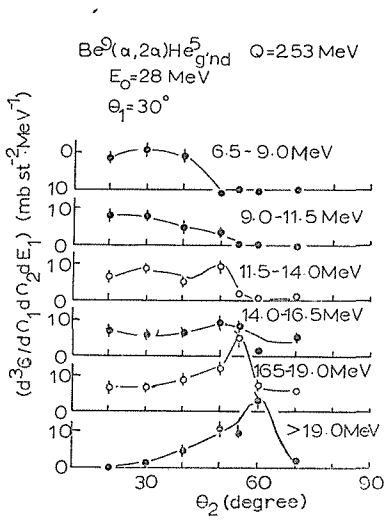

Fig. 14. The angular correlation distributions for the Be^9 (α, 2α) $He^5_{g'nd}$ ($Q\simeq -2.5$ MeV) reaction at 28.0 MeV obtained by the non-symmetric method when θ_1 is fixed at 30°. The distribution is shown for each 2.5 MeV interval of E_1.

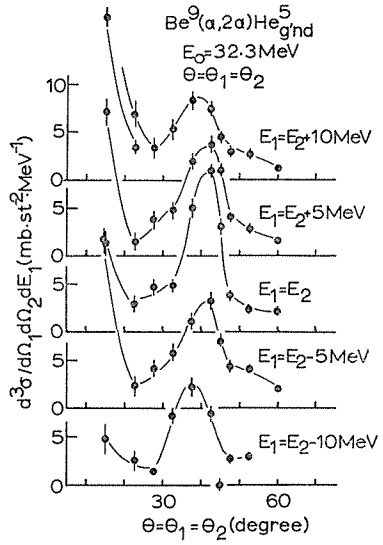

Fig. 15. The angular correlation distributions for the Be^9 (α, 2α) He^5 ($Q\simeq -2.5$ MeV) reaction at 32.3 MeV obtained by the symmetric method ($\theta=\theta_1=\theta_2$). The distribution is shown for each 5.0 MeV interval of E_1.

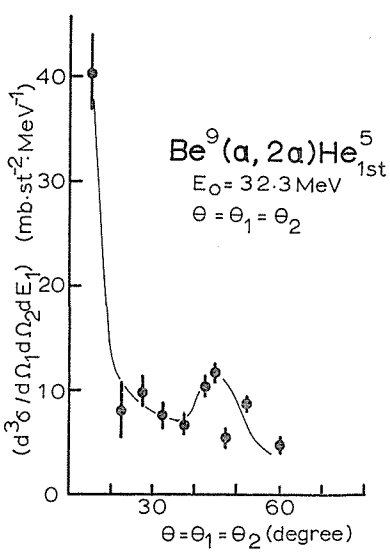

Fig. 16. The angular correlation distributions for the Be^9 (α, 2α) He^5_{1st} ($Q\simeq -7.0$ MeV) reaction at 32.3 MeV obtained by the symmetric method ($\theta=\theta_1=\theta_2$). Only the symmetric energy distribution ($E_1\simeq E_2$) is shown.

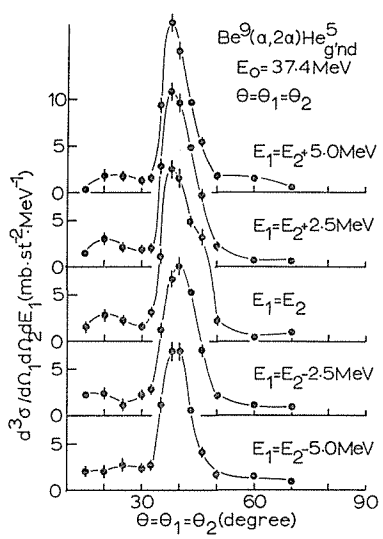

Fig 17. The angular correlation distributions for the Be^9 (α, 2α) $He^5_{g'nd}$ ($Q\simeq -2.5$ MeV) reaction at 37.4 MeV obtained by the symmetric method ($\theta=\theta_1=\theta_2$). The distributions is shown for each 2.5 MeV interval of E_1.

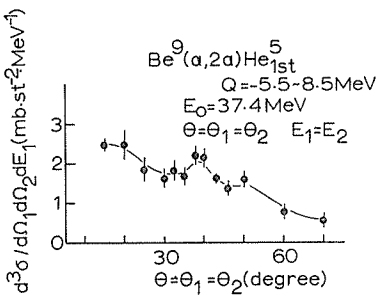

Fig. 18. The angular correlation distributions for the Be^9 (α, 2α) He^5_{1st} ($Q\simeq -7.0$ MeV) reaction at 37.4 MeV obtained by the symmetric method ($\theta=\theta_1=\theta_2$). Only the symmetric energy distribution ($E_1\simeq E_2$) is shown.

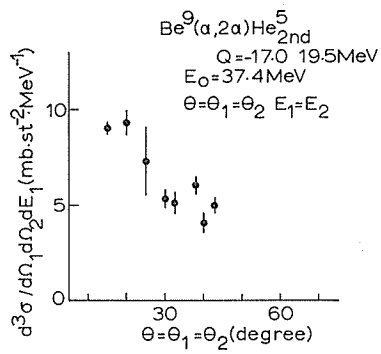

Fig. 19. The angular correlation distributions for the Be^9 (α, 2α) He^5_{2nd} ($Q\simeq -19.2$ MeV) reaction at 37.4 MeV obtained by the symmetric method ($\theta=\theta_1=\theta_2$). Only the symmetric energy distribution ($E_1\simeq E_2$) is shown.

obtained by the symmetric method at 37.4 MeV. In Fig. 17, the angular correlation distributions about the region of $Q\simeq -2.5$ MeV are shown for each 1.25 MeV interval of E_1. If $E_1\simeq E_2$, the recoilless angle is 43.0° and a maximum of the differential cross section is also observed at this angle. In Figs. 18 and 19, the angular correlation distributions of the alpha-particles about the regions around $Q\simeq -7.0$ MeV and -19.2 MeV are shown respectively.

An important fact is that, throughout the experiment, the differential cross section has a maximum at the recoilless angle. Another important fact is that the angular correlation distributions at the forward angles vary their shape with the change of the incident energy and the detection method. These facts are consistent with the quasi-free alpha-alpha scattering process as will be discussed later.

3.2. B^{10} (α, 2α) Li^6 Reaction

The summed energy spectrum is given in Fig. 20, where the abscissa represents the summed energy and the excitation energy of the residual Li^6 nucleus simultaneously. There exist apparently peaks at the Q value of about -4.5 MeV and about -6.6 MeV, which correspond to the ground and the 1 st excited states of Li^6. The angular correlation distributions are obtained about these two peaks.

Fig. 21 shows the angular correlation distribution of the alpha-particles about the region of $Q\simeq -4.5$ MeV obtained by the symmetric method ($\theta=\theta_1=\theta_2$) where $E_1\simeq E_2$. Fig. 22 shows the angular correlation distribution about the same region obtained by the non-symmetric method ($\theta_1=40°$ where $E_1\simeq E_2$). In Fig. 23, the angular correlation distribution of the alpha-particles about the region of $Q\simeq -6.6$ MeV is given.

In Figs. 21 and 22, the shape of the angular correlation distributions around the recoilless angle (40°) is quite different from that of Be^9 nucleus. The one reason is that the relative angular momentum state between an alpha-particle and a Li^6 core in B^{10} nucleus is different from that in Be^9. The other reason is the difference of the reaction Q-value. The sudden rise of the differential cross section in Fig. 22 at the backward angles is interpreted as the effect of the sequential alpha

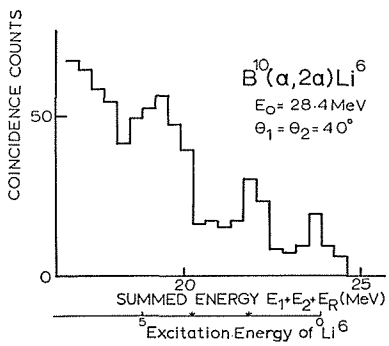

Fig. 20. A summed energy spectrum of the emitted alpha-particles from the B^{10} $(\alpha, 2\alpha)$ Li^6 reaction at 28.4 MeV when both counters are set at 40° $(=\theta_1=\theta_2)$.

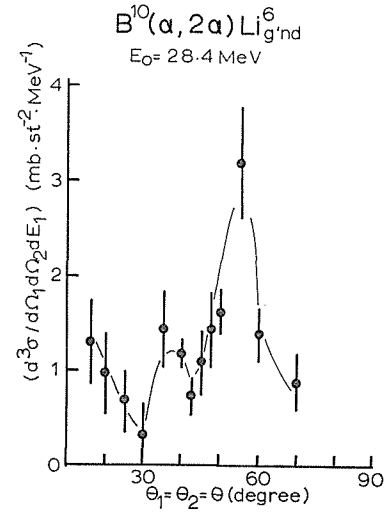

Fig. 21. The angular correlation distribution for the B^{10} $(\alpha, 2\alpha)$ $Li^6{}_{g'nd}$ ($Q\simeq -4.5$ MeV) reaction at 28.4 MeV obtained by the symmetric method ($\theta=\theta_1=\theta_2$). Only the symmetric energy distribution ($E_1\simeq E_2$) is shown.

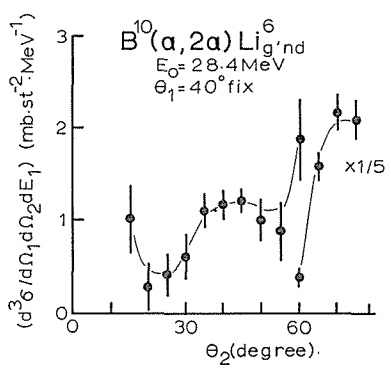

Fig. 22. The angular correlation distribution for the B^{10} $(\alpha\ 2\alpha)$ $Li^6{}_{g'nd}$ ($Q\simeq -4.5$ MeV) reaction at 28.4 MeV obtained by the non-symmetric method when θ_1 is fixed at 40°. Only the symmetric energy distribution ($E_1\simeq E_2$) is shown.

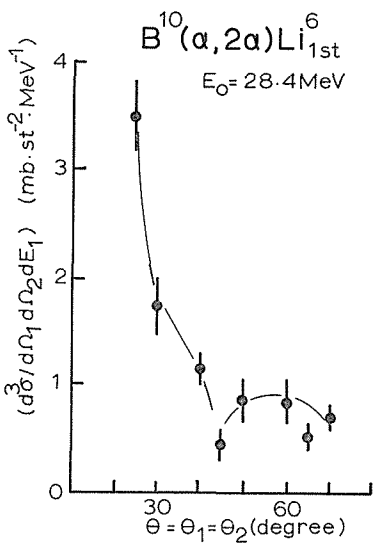

Fig. 23. The angular correlation distribution for the B^{10} $(\alpha, 2\alpha)$ $Li^6{}_{1st}$ ($Q\simeq -6.6$ MeV) reaction at 28.4 MeV obtained by the non-symmetric method at 40°.

decay process.

3.3. C^{12} $(\alpha, 2\alpha)$ Be^8 Reaction

Fig. 24 represents the summed energy spectra of the alpha-particles from C^{12} $(\alpha, 2\alpha)$ Be^8 reaction at 28.0 MeV and 37.4 MeV when both counters were set at the recoilless angles. Peaks are found at the Q-value of about -7.5 MeV and about -10.3 MeV, which correspond to the ground and the 1 st excited state of Be^8.

Figs. 25~29 show angular correlation distributions at 28.0 MeV. The angular correlation distribution about $Q\simeq -7.5$ MeV are shown for each 2.5 MeV intervals of E_1. Figs. 25 and 26 give the results obtained by the symmetric method and the non-symmetric method ($\theta_1=35°$) respectively. The recoilless angle is 35° ($=\theta=\theta_1=\theta_2$) if $E_1\simeq E_2$. This condition is held when E_1 is 9.5 MeV -11.5 MeV. The shapes of the angular correlation distributions around the recoilless angle are quite different from that of Be^9. This fact is concerned to the difference of the reaction Q value (i. e. -7.5 MeV), as will be discussed later. Figs. 27 and 28 give the results obtained by the non-symmetric method when θ_1 was fixed at 25° and 50° respectively. The recoilless points are not included in these figures.

Figs. 30 and 31 show the angular correlation distributions obtained by the symmetric method at 37.4 MeV. The former gives the results for the region of $Q\simeq -7.5$ MeV and the latter for the region of $Q\simeq -10.3$ MeV. In Fig. 27, the

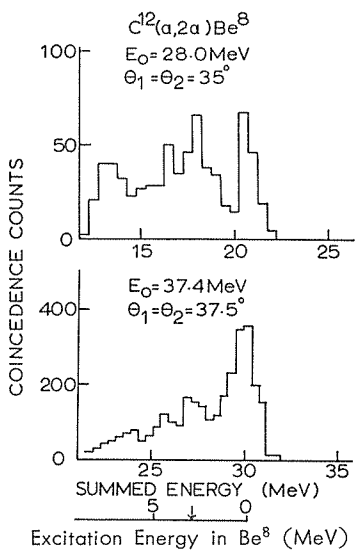

Fig. 24. The summed-energy spectra of the emitted alpha-particles from the C^{12} $(\alpha, 2\alpha)$ Be^8 reaction at 28.0 and 37.4 MeV respectively, when both counters are set at the recoilless angles for the Q-value of -7.5 MeV in the symmetric method. The abscissa shows the summed energy $(E_1+E_2+E_R)$ and the excitation energy of the residual Be^8 nucleus.

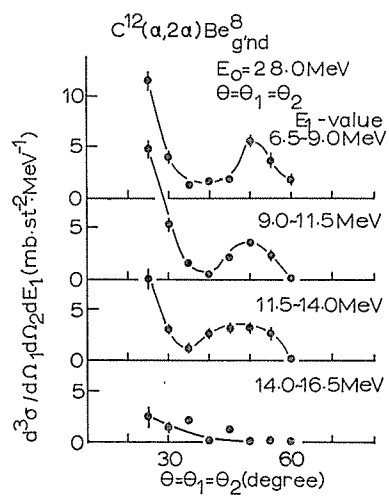

Fig. 25. The angular correlation distributions for the C^{12} $(\alpha, 2\alpha)$ $Be^8{}_{g'nd}$ $(Q\simeq -7.5$ MeV) reaction at 28.0 MeV obtained by the symmetric method ($\theta=\theta_1=\theta_2$). The distribution is shown for each 2.5 MeV interval of E_1.

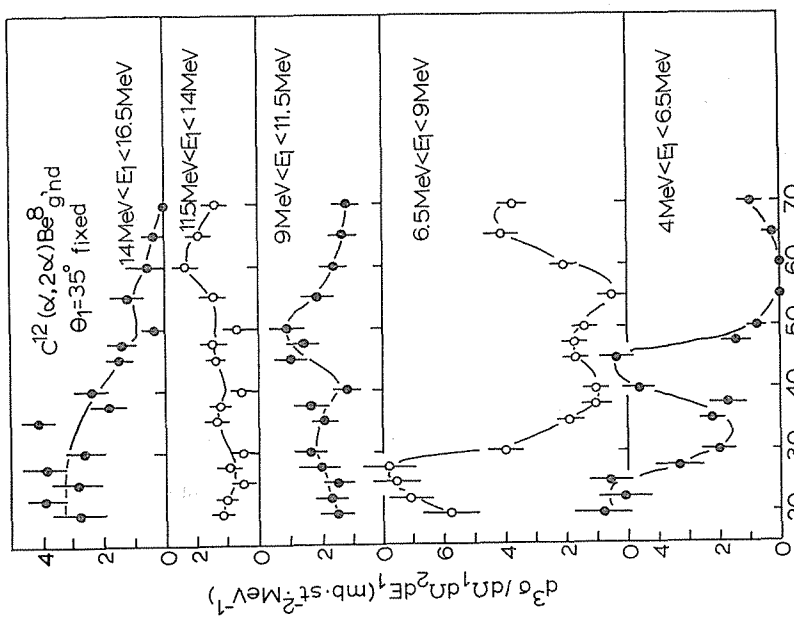

Fig. 26. The angular correlation distributions for the C^{12} $(\alpha, 2\alpha)$ $Be^{8}{}'_{g.nd}$ ($Q \simeq -7.5$ MeV) reaction at 28.0 MeV obtained by the non-symmetric method at 35°. The distribution is shown for each 2.5 MeV interval of E_1.

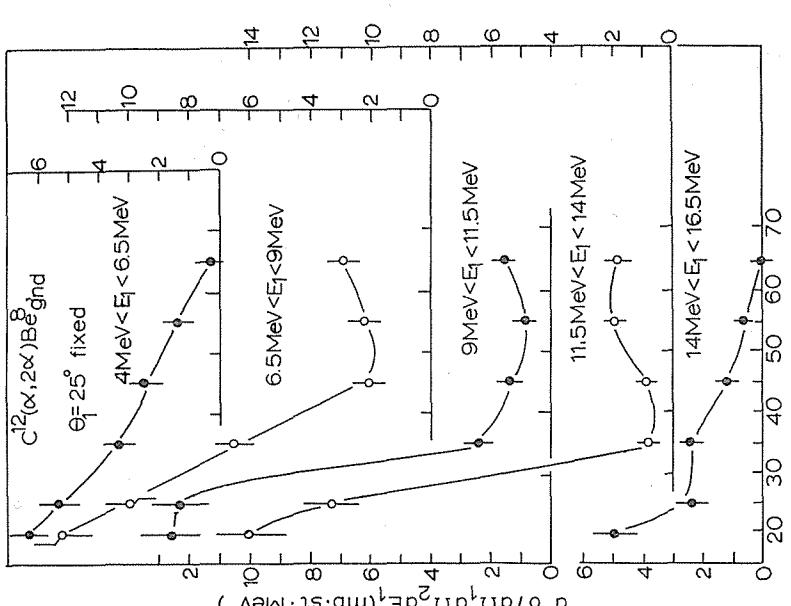

Fig. 27. The angular correlation distributions for the C^{12} $(\alpha, 2\alpha)$ Be^{8} ($Q \simeq -7.5$ MeV) reaction at 28.0 MeV obtained by the non-symmetric method when θ_1 is fixed at 25°. The distribution is shown for each 2.5 MeV interval of E_1.

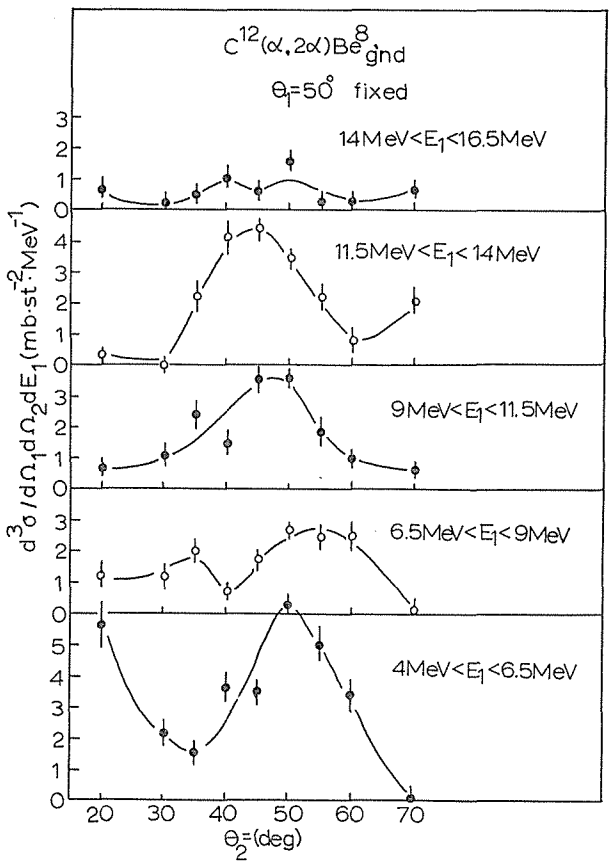

Fig. 28. The angular correlation distributions for the C^{12} $(\alpha, 2\alpha)$ $Be^{8}g'_{nd}$ ($Q\simeq -7.5$ MeV) reaction at 28.0 MeV obtained by the non-symmetric method when θ_1 is fixed at 50°. The distribution is shown for each 2.5 MeV interval of E_1.

recoilless point is $\theta=\theta_1=\theta_2=35°$, and $E_1\simeq E_2$. Also in this case the shape of the distribution is different from that of Be^9 nucleus. The large Q value is the reason of the distortion of the shape of the distribution.

3.4. O^{16} $(\alpha, 2\alpha)$ C^{12} Reaction

The summed energy spectrum is given in Fig. 32. The abscissa shows the summed energy and the excitation energy of the residual C^{12} nucleus. A sharp peak is observed in the vicinity of the ground state of C^{12} nucleus ($Q\simeq -7.2$ MeV). Fig. 33 gives the angular correlation distribution for the region of $Q\simeq -7.2$ MeV obtained by the symmetric method at 26.5 MeV. The recoilless angle is 34° $(=\theta=\theta_1=\theta_2)$.

3.5. Be^9 $(p, p\alpha)$ He^5 Reaction

Fig. 34, shows a two-dimensional energy spectrum of protons and alpha-particles from the reaction Be^9 $(p, p\alpha)$ He^5 at 55°$(=\theta_p=\theta_\alpha)$ and at 55 MeV. Because

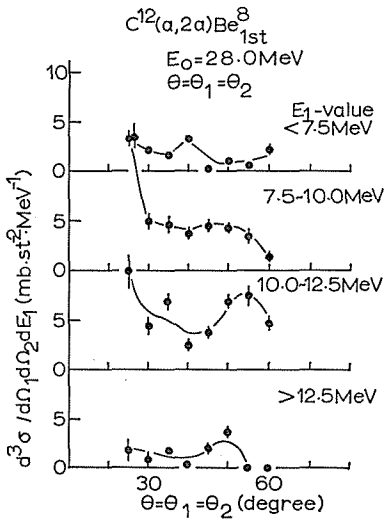

Fig. 29. The angular correlation distributions for the C^{12} $(\alpha, 2\alpha)$ Be^{8}_{1st} ($Q \simeq -10.3$ MeV) reaction at 28.0 MeV obtained by the symmetric method ($\theta=\theta_1=\theta_2$). The distribution is shown for each 2.5 MeV interval of E_1.

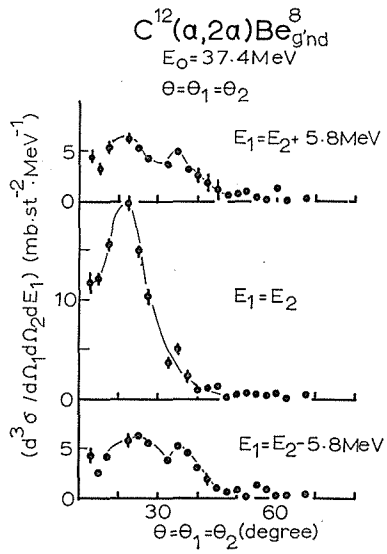

Fig. 30. The angular correlation distributions for the C^{12} $(\alpha, 2\alpha)$ $Be^{8}_{g'nd}$ ($Q \simeq -7.5$ MeV) reaction at 37.4 MeV obtained by the symmetric method ($\theta=\theta_1=\theta_2$). The distribution is shown for each 5.8 MeV interval of E_1.

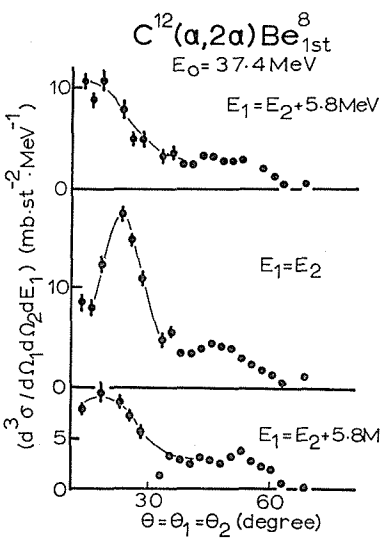

Fig. 31. The angular correlation distributions for the C^{12} $(\alpha, 2\alpha)$ Be^{8}_{1st} ($Q \simeq -10.3$ MeV) reaction at 37.4 MeV obtained by the symmetric method ($\theta=\theta_1=\theta_2$). The distribution is shown for each 5.8 MeV interval of E_1.

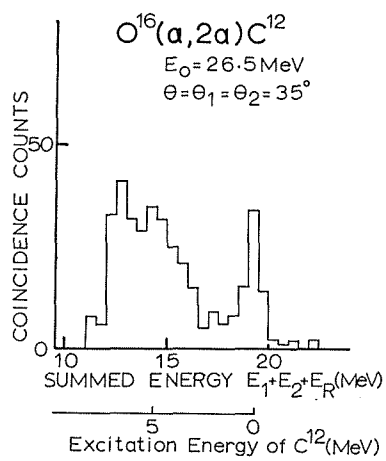

Fig. 32. A summed-energy spectrum of the emitted alpha-particles from the O^{16} $(\alpha, 2\alpha)$ C^{12} reaction at 26.5 MeV, when both counters are set at 35° ($=\theta_1=\theta_2$).

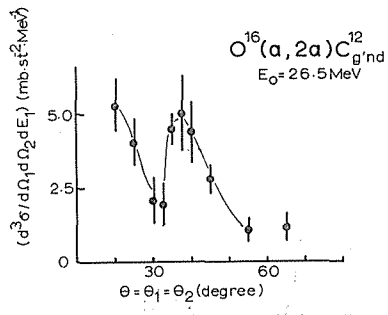

Fig. 33. The angular correlation distribution for the O^{16} $(\alpha, 2\alpha)$ $C^{12}{}_{g'nd}$ $(Q\simeq -7.3$ MeV) reaction at 26.5 MeV obtained by the symmetric method $(\theta=\theta_1=\theta_2)$. Only the symmetric energy distribution $(E_1\simeq E_2)$ is shown.

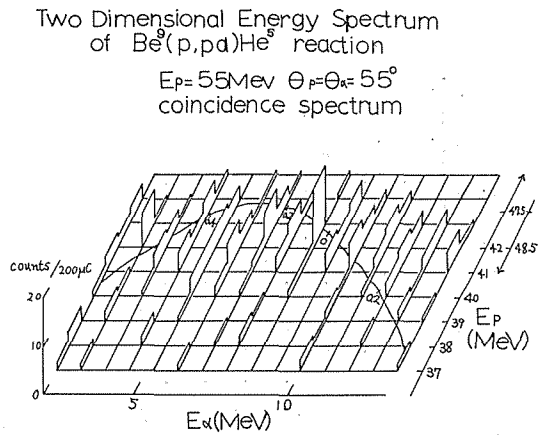

Fig. 34. A two-dimensional energy spectrum of protons and alpha-particles from the reaction Be^9 $(p, p\alpha)$ He^5 at 55°$(=\theta_p=\theta_\alpha)$ and at 55 MeV.

protons of higher than 47.5 MeV penetrated the detector, the proton energy scale in the figure turns down at 47.5 MeV. However, a group of counts is observed around a line in this figure which corresponds to the ground state of the residual He^5 nucleus. In the figure a cross mark labeled "O" is a reciolless point. The angular correlation distributions was obtained by the symmetric momentum method $(\theta_p=\theta_\alpha, \hbar|\boldsymbol{k}_p|=\hbar|\boldsymbol{k}_\alpha|)$ for the region around the energy corresponding to the reaction Q-value of about -2.5 MeV. The width of the region is 7 MeV for E_p and 3.5 MeV for E_α. The result is given in Fig. 35. A maximum of the differential cross section was observed around the recoilless angle in spite of the poor statistics. This fact is consistent with the results of the $(\alpha, 2\alpha)$ reaction described in Section 3. 1. The absolute value of the differential cross section will be discussed later in connection with that of the $(\alpha, 2\alpha)$ reaction and may give further proof of the reaction mechanism.

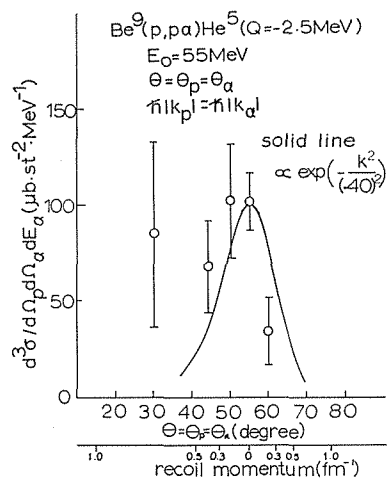

Fig. 35. The angular correlation distribution for the Be^9 $(p, p\alpha)$ $He^5{}_{g'nd}$ $(Q\simeq -2.5$ MeV) reaction at 55 MeV obtained by the symmetric momentum method $(\theta_p=\theta_\alpha, \hbar|\boldsymbol{k}_p|=\hbar|\boldsymbol{k}_\alpha|)$. The solid curve represents the calculated angular correlation distribution by using the momentum distribution function derived from the data of the Be^9 $(\alpha, 2\alpha)$ $He^5{}_{g'nd}$ reaction.

4. Discussion

4.1. The Direct Interaction Process

4.1.1. *General*

A quasi-free $x-\alpha$ scattering experiment, when both outgoing particles are detected with good energy and angular resolution, gives the information sufficient to determine the recoil momentum $\hbar\boldsymbol{k}_R$. The separation energy of an alpha-particle from the target nucleus is also determined. Then the information on the state in which an alpha-particle is coupled with the core in the target nucleus is given.

It is concluded from the experimental results in Section 3, that the quasi-free scattering is a good description for the reaction mechanism especially for Be^9. Therefore, it is worthwhile to analyse the experimental results with the direct interaction mechanism in the first place.

We use the impulse approximation for the description of this process, that is, an alpha-particle in a target nucleus is assumed to be knocked-out by an incident particle giving little effect on the core. In addition, we neglect the distortion of the incident and the outgoing waves by the core. The general expression for the cross section of the $(\alpha, 2\alpha)$ reaction is

$$\frac{d^9\sigma}{d^3\boldsymbol{k}_1 d^3\boldsymbol{k}_2 d^3\boldsymbol{k}_R} = \frac{4\pi^2 M_\alpha}{\hbar^2 k_0} |t_{fi}|^2 \delta^3(\boldsymbol{k}_1+\boldsymbol{k}_2+\boldsymbol{k}_R-\boldsymbol{k}_0) \times \delta(E_1+E_2+E_R+E_s-E_0). \quad \cdots\cdots(6)$$

M_α is the mass of an alpha particle and t_{fi} is the matrix element of the transition between the initial state and the final state.

In the first Born approximation and using plane waves for the wave function of the incident and outgoing particles, the matrix element t_{fi} can be represented as

$$t_{fi} = \frac{2\pi}{(M_\alpha c^2)^2} \sum_n g^{(n)}_{A-4,A}(\boldsymbol{k}_3) \cdot M(1, 2; 0, 3), \quad \cdots\cdots(7)$$

where $\hbar\boldsymbol{k}_3$ $(=\hbar\boldsymbol{k}_1+\hbar\boldsymbol{k}_2+\hbar\boldsymbol{k}_0)$ equals $-\hbar\boldsymbol{k}_R$ and becomes the same with the momentum $\hbar\boldsymbol{k}$ of the alpha cluster relative to the core in the nucleus.

$M(1, 2; 0, 3)$ is the matrix element corresponding to the scattering process of free alpha particles with the initial momenta $\hbar\boldsymbol{k}_0$, $\hbar\boldsymbol{k}_3$ and with the final momenta $\hbar\boldsymbol{k}_1$, $\hbar\boldsymbol{k}_2$, and relates to the free $\alpha-\alpha$ scattering cross section in the center of mass system, using the first Born approximation, as follows:

$$\frac{d\sigma}{d\bar{\Omega}}^{fr}(\bar{1}, \bar{2}; \bar{0}, \bar{3}) = \frac{1}{4}\left(\frac{2\pi}{\hbar c}\right)^4 \frac{1}{\bar{E}_0^2} |M(1, 2; 0, 3)|^2, \quad \cdots\cdots(8)$$

where barred quantities are taken in the center of mass system. $d\sigma/d\bar{\Omega}^{fr}$ $(\bar{1}, \bar{2}; \bar{0}, \bar{3})$ is the cross section of the free $\alpha-\alpha$ scattering not on the energy shell but off the energy shell.

$\sum_n |g^{(n)}_{A-4,A}(\boldsymbol{k}_3)|^2$ describe the relative momentum distribution of the alpha cluster in the nucleus, i. e., the probability of finding an alpha cluster in a state of momentum $\hbar\boldsymbol{k}$.

Using Eqs. (6), (7) and (8), the differential cross section is expressed as follows:

$$\frac{d^4\sigma}{dE_1 d\Omega_1 dE_2 d\Omega_2} = \frac{M_\alpha k_1 k_2}{\hbar^2 k_0} \sum_n |g^{(n)}_{A-4,A}(\boldsymbol{k}_3)|^2$$

$$\times \frac{d\sigma}{d\Omega}^{pr}(\vec{1},\ \vec{2};\ \vec{0},\ \vec{3})\cdot\delta(E_1+E_2+E_R+E_s-E_0) \qquad \cdots\cdots(9)$$

Then we assume the cluster structure of the nucleus and represent the wave function for the target nucleus as follows:

$$\psi_A=N\sum_{LM}\phi_\alpha(\boldsymbol{r}_1)\phi_{A-4}(\boldsymbol{r}_3)\chi_{LM}(\boldsymbol{R}) \qquad \cdots\cdots(10)$$

Here, $\phi_\alpha(\boldsymbol{r}_1)$ is the internal wave function for the alpha cluster in the nucleus. $\phi_{A-4}(\boldsymbol{r}_3)$ is the internal wave function for the rest part of the nucleus in a certain state of the residual nucleus. $\chi_{LM}(\boldsymbol{R})$ is the wave function for the relative motion between the alpha cluster and the core in the target nucleus. Here, we spproximate $\chi_{LM}(\boldsymbol{R})$ by the following equation:

$$\left.\begin{aligned}\chi_{LM}(\boldsymbol{R})&=N_L\cdot\chi(R)Y_{LM}(\Omega),\\ \chi(R)&=R^n\exp\left[-\frac{1}{2}\beta R^2\right],\\ \boldsymbol{R}&=\boldsymbol{r}_1-\boldsymbol{r}_3,\end{aligned}\right\} \qquad \cdots\cdots(11)$$

where β is the parameter which relates to the spacial spread of the relative motion. L is the relative angular momentum between the alpha cluster and the core. The Gauss type function is assumed for $\chi(R)$ in order to simplify the calculation as is usually done.[3,4,5] N is the normalization constant for the totaly system. In the wave function (10), we neglect the antisymmetrization, which has little effect, if the alpha cluster is thoroughly separated spacially from the core in the nucleus. This extreme approximation is convenient to see the situation at first sight. Then, the normalization constant N of the target wave function is used to normalize only the wave function of the relative motion $\chi_{LM}(\boldsymbol{R})$, assuming $\phi_\alpha(\boldsymbol{r}_1)$ and $\phi_{A-4}(\boldsymbol{r}_3)$ are the normalized wave functions.

Then the momentum distribution becomes

$$\sum_n|g^{(n)}_{A-4,A}(\boldsymbol{k})|^2=\sum_{LM}\frac{N_\alpha}{2L+1}\left|\int e^{i\boldsymbol{k}\cdot\boldsymbol{R}}\chi_{LM}(\boldsymbol{R})d\boldsymbol{R}\right|^2$$
$$\times\left|\int\phi^*_\alpha(\boldsymbol{r}_1)\phi^*_{A-4}(\boldsymbol{r}_3)\phi_\alpha(\boldsymbol{r}_1)\phi_{A-4}(\boldsymbol{r}_3)d\boldsymbol{r}_1d\boldsymbol{r}_3\right|^2 \qquad \cdots\cdots(12)$$

where ψ_α and ψ_{A-4} are the internal wave functions of the alpha particle and the residual nucleus, respectively, in the free space.

In Eq. (12), the last factor on the right is often interpreted as the probability of finding the alpha cluster in the nucleus and the first factor as a normalized momentum density distribution.[26] Here we put them as follows.

$$P_\alpha=\left|\int\phi^*_\alpha(\boldsymbol{r}_1)\phi^*_{A-4}(\boldsymbol{r}_3)\phi_\alpha(\boldsymbol{r}_1)\phi_{A-4}(\boldsymbol{r}_3)d\boldsymbol{r}_1d\boldsymbol{r}_3\right|^2 \qquad \cdots\cdots(13)$$

$$\rho_L(\boldsymbol{k})=N_L^2\cdot\sum_M\left|\int e^{-i\boldsymbol{k}\cdot\boldsymbol{R}}\chi_{LM}(\boldsymbol{R})d\boldsymbol{R}\right|^2 \qquad \cdots\cdots(14)$$

Then,

$$\sum_n|g^{(n)}_{A-1,A}(\boldsymbol{k})|^2=f(\boldsymbol{k})=\sum_L N_L^2\cdot P_\alpha\cdot\rho_L(\boldsymbol{k}) \qquad \cdots\cdots(15)$$

In the actual calculation, the most simple function is used as $f(\boldsymbol{k})$, that is,

$$f_L(\boldsymbol{k})=P\cdot\left(\frac{\boldsymbol{k}}{\alpha}\right)^{2L}\exp\left[-\left(\frac{\boldsymbol{k}}{\alpha}\right)^2\right], \qquad \cdots\cdots(16)$$

corresponding to each relative angular momentum state. In this equation α is

relevant to the spacial spread of the relative motion, where $\alpha=\sqrt{2\beta}$. P is the amplitude of the momentum distribution and is equal to the product of N_L^2 and P_α and the factor due to the transformation to the momentum space.

In the case of the $(p, p\alpha)$ reaction, the differential cross section is expressed, similarly to the equation (9), as follows:

$$\frac{d^4\sigma}{dE_p d\Omega_p dE_\alpha d\Omega_\alpha}=\frac{M_\alpha k_p k_\alpha}{\hbar^2 k_0}\sum_n |g^{(n)}_{A-4,A}(\boldsymbol{k}_3)|^2 \times\frac{d\sigma}{d\bar{\Omega}}^{fr}(\bar{p}.\ \bar{\alpha};\ \bar{0},\ \bar{3})\cdot\delta(E_p+E_\alpha+E_R+E_s-E_0) \quad\cdots\cdots(17)$$

In the actual calculation, we use the function expressed by Eq. (16) as in the case of the $(\alpha, 2\alpha)$ reaction. When there exists the distortion of the incident or the outgoing wave, i. e., when the interaction between the incoming or outgoing particle and the core cannot be negligible, the situation is different. When the incoming and the outgoing wave are affected by the corresponding optical potentials, which, are not so different each other, the momentum distribution function $\sum_n |g^{(n)}_{A-4,A}(\boldsymbol{k}_3)|^2$ is distorted. If analogy with the calculation about the quasi-free proton-proton scattering can be held, the amplitude of the momentum distribution is strongly decreased and the shape is relatively smeared out.[21] However the accurate distorted wave treatment of the quasi-free scattering process is not easy at present from some theoretical reasons.[22] Then, we make bold to neglect the distortion effect in order to see the essential qualities of the phenomena.

The cross section Eq. (8), cannot be accurately estimated, because we have no experimental data about the scattering off-the-energy-shell. So, we must choice a conventional method. We replace the value of $d\sigma/d\bar{\Omega}^{fr}(\bar{1},\ \bar{2};\ \bar{0},\ \bar{3})$, by the experimental differential cross section on the energy shell for the same amount of momentum transfer $(=\hbar\{(\boldsymbol{k}_0-\boldsymbol{k}_3)-(\boldsymbol{k}_1-\boldsymbol{k}_2)\})$ at the incident energy of $\hbar^2|\boldsymbol{k}_0-\boldsymbol{k}_3|^2/2M_\alpha$. This convenient method is usually employed in the treatment of the nucleon-nucleon scattering off the energy shell[23] and is proved very feasible. In the case of the Be^9 $(\alpha, 2\alpha)$ He^5 reaction the value obtained by this method is not so far apart from the theoretically calculated one by using a phenomenological potential of alpha-alpha interaction.[25]

4. 1. 2. Be^9 *Nucleus*

Fig. 36 shows the calculated angular correlation distribution, following the above mentioned methed, together with the experimental values for the Be^9 $(\alpha, 2\alpha)$ He^5 reaction. The spin-parity of the ground state of Be^9 is $3/2-$, that of the ground state of He^5 is $3/2-$, and that of the alpha-particle is $0+$, so the relative angular momentum between alpha-particle and He^5 in Be^9 is $L=0, 2$. We consider the relative S state only and put $f(\boldsymbol{k})=P\cdot\exp[-(\boldsymbol{k}/\alpha)^2]$. In the figure the calculated angular correlation distribution is given for three values of α, and as seen in the fignre the distribution is sensitive to the parameter α. $\alpha=0.40\ \mathrm{fm}^{-1}$ is the best as seen in the figure. Then, $P=0.88\ \mathrm{fm}^3\cdot\mathrm{st}^{-1}$. As a result the momentum distribution of an alpha-cluster in Be^9 is given by a function $f(\boldsymbol{k})=0.88\exp[-\boldsymbol{k}^2/(0.40)^2]$. This function reproduces the four kinds of the angular correlation distribution fairly well, i. e. this function reproduces not only the peak around the recoilless angle but also the variation of the differential cross section at the forward angles. This variation is just in accord with the variation of the differential cross section

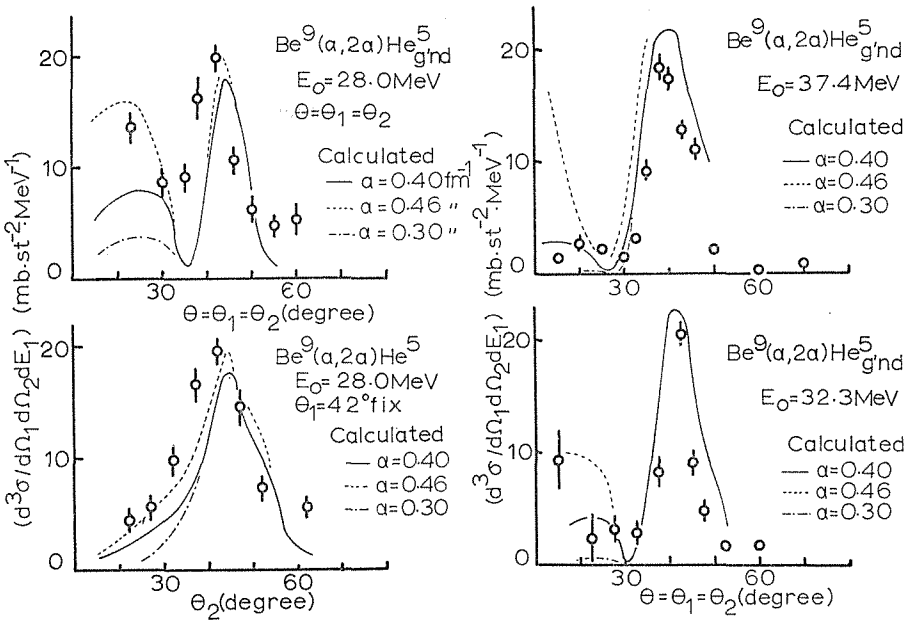

Fig. 36. The calculated angular correlation distributions together with the experimental values for the Be^9 $(\alpha, 2\alpha)$ $He^5_{g'nd}$ reaction. The experimental angular correlation distribution in this figure are that obtained by the symmetric method ($\theta_1=\theta_2$) and when $E_1\simeq E_2$ at each energy and that obtained by the non-symmetric method ($\theta_1=42°$) and when $E_1\simeq E_2$ at 28.0 MeV. For calculations and discussions see in text.

of the free alpha-alpha scattering. The spread of the momentum distribution is so narrow and the amplitude is so large, that the existence of the strong alpha-clustering correlation in Be^9 is clear.

The momentum distribution function $f(\boldsymbol{k})$ used in the analysis of the $(\alpha, 2\alpha)$ reaction on Be^9 is used also for the angular correlation distribution from the Be^9 $(p, p\alpha)$ He^5 reaction. The calculated angular correlation distribution is shown in Fig. 35 where the absolnte value is normalized at the recoilless angle, and fits well the experimental value. In order to ckeck the grade of the fit of the absolute value, the ratio of the cross section of the $(\alpha, 2\alpha)$ reaction to that of the $(p, p\alpha)$ reaction is given at the recoilless angle for both the experimental and the calculated, as follows: The result is

$$\frac{\left(\dfrac{d^3\sigma}{d\Omega_1 d\Omega_2 dE_1(\alpha-2\alpha)}\right)_{\text{exp.}}}{\left(\dfrac{d^3\sigma}{d\Omega_p d\Omega_\alpha dE_\alpha(p-p\alpha)}\right)_{\text{exp.}}}=(1.92\pm0.33)\times10^2$$

and

$$\frac{\left(\dfrac{d^3\sigma}{d\Omega_1 d\Omega_2 dE_1(\alpha-2\alpha)}\right)_{\text{cal.}}}{\left(\dfrac{d^3\sigma}{d\Omega_p d\Omega_\alpha dE_\alpha(p-p\alpha)}\right)_{\text{cal.}}}=1.03\times10^2$$

They are in good accordance and give support to our treatment.

4. 1. 3. B^{10} *Nucleus*

The spin-parity of the ground state of Li^6 is 1+, that of the alpha-particle is 0+, and that of B^{10} is 3+, so the relative angular momentum is $L=2$ and 4. We consider only the relative D state and put $f(\boldsymbol{k})=P\cdot(\boldsymbol{k}/\alpha)^4\exp[-(\boldsymbol{k}/\alpha)^2]$. In Fig. 37, the calculated angular correlation disributions are shown together with the experimental value for the B^{10} (α, 2α) Li^6 reaction. When $\alpha=0.57\,f^{-1}$, $P=0.83$ $fm^3\cdot st^{-1}$, a good fit is obtained. However, in the region coresponding to the large momentum of the cluster, the fit is not so good. In this region, the effect of the distortion is considered to be large for the D state, so the plane wave approximation is not sufficient. The experiments at different energies may clarify this situation.

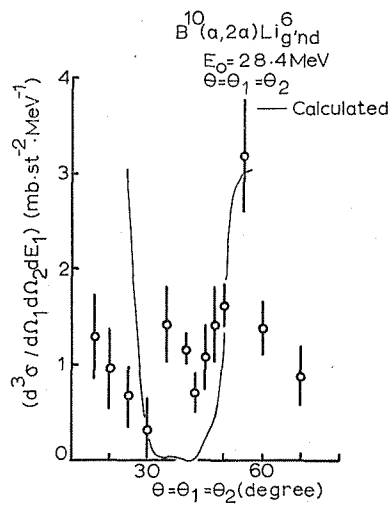

Fig. 37. The calculated angular correlation distribution together with the experimental values for the B^{10} (α, 2α) $Li^6{}_{g'nd}$ ($Q\simeq-4.5$ MeV) reaction. The experimental angular correlation distribution in this figure is that obtained by the symmetric method ($\theta_1=\theta_2$) and when $E_1\simeq E_2$ at 28.4 MeV. For calculations and discussions see in text.

4. 1. 4. C^{12} *Nucleus*

The spin-parity of the ground state of C^{12} is 0+. that of Be^8 is 0+ and that of an alpha-particle is 0+, so the relative angular momentum between alpha-particle and Be^8 in C^{12} is only $L=0$. We put $f(\boldsymbol{k})=P\cdot\exp[-\boldsymbol{k}^2/\alpha^2]$. When $\alpha=0.80\,f^{-1}$ and $P=0.036\,fm^3\cdot st^{-1}$, a good fit is obtained. The calculated angular correlation distribution is given in Fig. 38 together with the experimental values for the C^{12} (α, 2α) Be^8 reaction. The experimental angular correlation distributions have not a maximum but rather a dip around the recoilless angle. This distribution seems inconsistent at a glance with assumption of the S-state distribution, but can be reproduced rather well when one takes into account the variation of the differential cross section of the free alpha-alpha scattering. The reaction Q-value of the C^{12} (α, 2α) Be^8 reaction is much larger than that of the Be^9 (α, 2α) He^5 reaction,

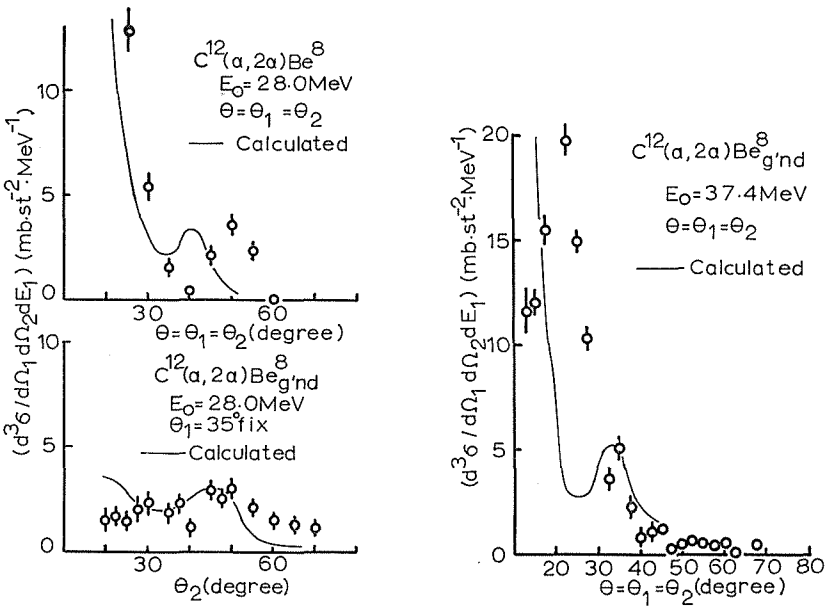

Fig. 38. The calculated angular correlation distributions for the C^{12} $(\alpha, 2\alpha)$ $Be^{8}_{g'nd}$ ($Q\simeq -7.5$ MeV) reaction. The experimental angular correlation distributions in this figure are those obtained by the symmetric method ($\theta_1=\theta_2$) and when $E_1\simeq E_2$ at both energies that obtained by the non-symmetric method ($\theta_1=35°$) when $E_1\simeq E_2$ at 28.0 MeV. For calculations and discussions see in text.

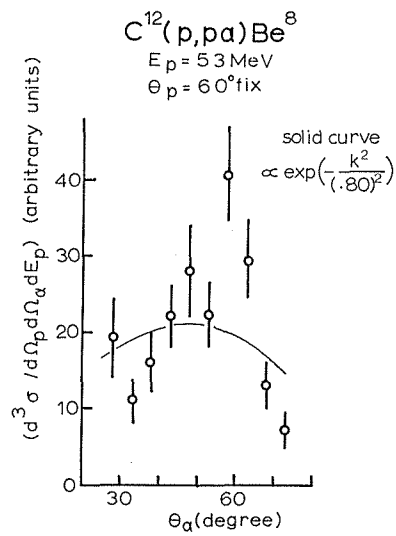

Fig. 39. The angular correlation distridution of the C^{12} $(p, p\alpha)$ Be^{8} reaction at 53 MeV reported in Ref. (27). The solid curve represents the calculated angular correlation distribution by using the momentum distribution function derived from the data of the C^{12} $(\alpha, 2\alpha)$ $Be^{8}_{g'nd}$ reaction.

so that off-the-energy shell effect is larger. In the C^{12} (α, 2α) Be^8 reaction experiment, there may be the effect of the sequential two-body decay process as will be stated in the next section. These two facts may be the reasons that fits are not so well. About the momentum distribution functions, it should be noted that the value of parameter α is two times larger than those for Be^9, B^{10} and O^{16}.

The momentum distribution function thus decided is applied to the experimental data of the C^{12} (p, $p\alpha$) Be^8 reaction at E_p=53 MeV.[27] The spread of the momentum distributions is similar as seen in Fig. 39.

4.1.5. O^{16} *Nucleus*

The spin-parity of the grond state of O^{16} is 0+, that of the ground state of C^{12} is 0+ and that of the alpha-particle is 0+, so the relative angular momentum between alpha-particle and C^{12} in O^{16} is only L=0. We put $f(\boldsymbol{k})=P\cdot\exp[-k^2/\alpha^2]$. The calculated angular correlation distribution is given in Fig. 40 together with the experimental value for the O^{16} (α, 2α) C^{12} reaction. When α=0.34 f^{-1}, P=0.51 $fm^3\cdot st^{-1}$, a good fit is obtained. The dip around θ=35° is explained by the variation of the differential cross section of the free alpha-alpha scattering. The spread of the momentum distribution thus obtained is considerably narrow.

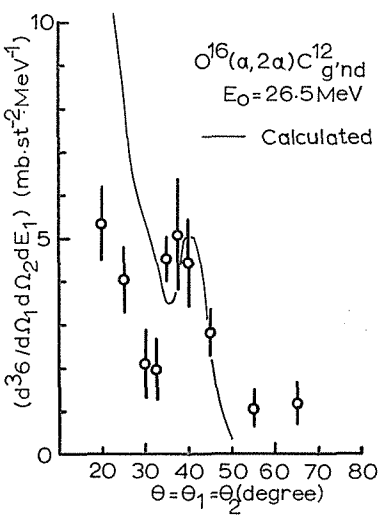

Fig. 40. The calculated angular correlation distribution for the O^{16} (α, 2α) $C^{12}{}_{g'nd}$ ($Q\simeq-7.3$ MeV) reaction. The experimental angular correlation distribution in this figure is that obtained by the symmetric method ($\theta_1=\theta_2$) and when $E_1\simeq E_2$ at 26.5 MeV. For calculation and discussion see in text.

4.2. The Sequential Decay Process

In such a nuclear reaction that contains three particles in its final state the sequential two-body decay process must be taken into account besides the quasi-free scattering process.[28] In this process, the reaction proceed via two independent steps, for instance, excitation of the target nucleus and its subsequant decay. In the (α, 2α) reaction, following process can be considered: in the first step, an

incident alpha-particle is inelastically scattered by the target nucleus and the target nucleus is left in an excited state with sufficiently long-life, and, in the second step, the excited nucleus emits an alpha-particle. This sequential decay process can be selected out following the kinematical condition. The energy of an inelastically scattered alpha-particle at an angle is decided from the excitation energy of the recoiled nucleus. When an inelastically scattered alpha particle is detected by a

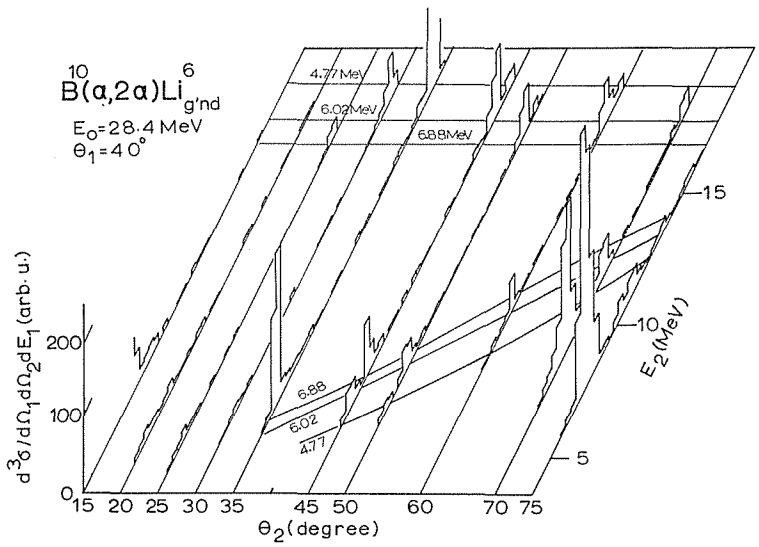

Fig. 41. The $E_1-\theta_2$ correlation distribution for the B^{10} $(\alpha, 2\alpha)$ $Li^6{}_{g'nd}$ ($Q\simeq -4.5$ MeV) reaction at 28.4 MeV when θ_1 is fixed at 40°. The solid lines show the energies of the alpha-particles corresponding to the sequential decay process.

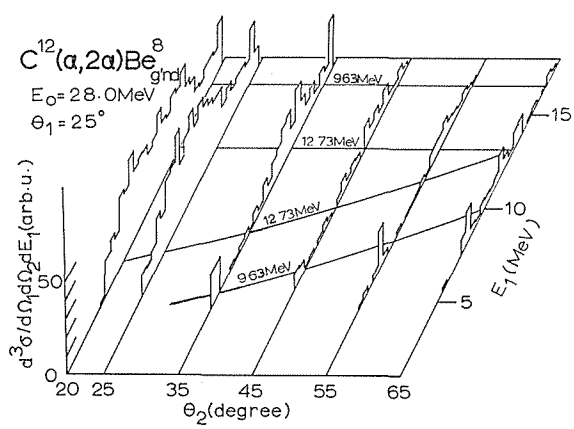

Fig. 42. The $E_1-\theta_2$ correlation distribution for the C^{12} $(\alpha, 2\alpha)$ $Be^8{}_{g'nd}$ ($Q\simeq -7.5$ MeV) reaction at 28.0 MeV when θ_1 is fixed at 35°. The solid lines show the energies of the alpha-particles corresponding to the sequential decay process.

counter at a fixed angle and the subsequently emitted alpha particle is detected by another counter which varies its angle, the energy of the former is constant whatever is the detection angle of the latter.

To see the mixing of the sequential decay process, we measured the angular correlation distribution in which one counter is fixed and another is varied. An angular correlation distribution of the B^{10} (α, 2α) Li^6 reaction, when counter 1 is fixed at 40° and counter 2 varies its angle, is shown in Fig. 41. The differential cross section is shown in the $E_1-\theta_2$ plane. Peaks corresponding to some excited states of B^{10} are found as indicated in the figure. It seems that the alpha particles from the sequential decay process are not contained so much in the region where

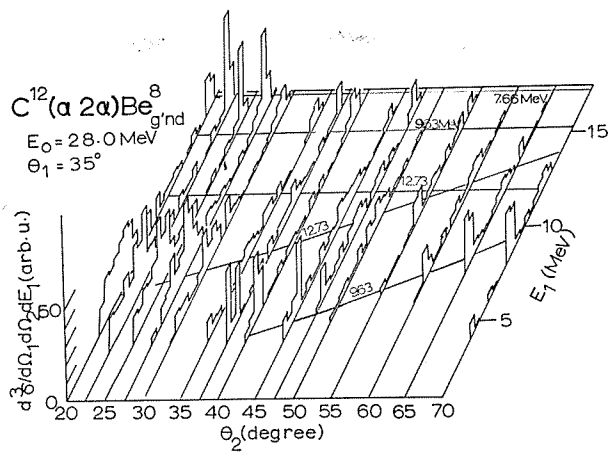

Fig. 43. The $E_1-\theta_2$ correlation distribution for the C^{12} (α, 2α) Be^8g'nd ($Q\simeq -7.5$ MeV) reaction at 28.0 MeV when θ_1 is fixed at 35°. The solid lines show the energies of the alpha-particles corresponding to the sequential decay process.

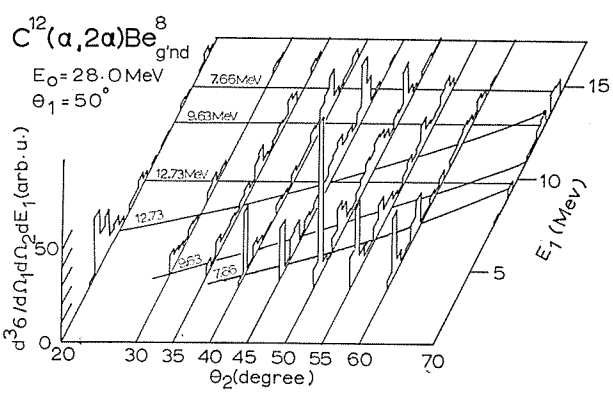

Fig. 44. The $E_1-\theta_2$ correlation distribution for the C^{12} (α, 2α) Be^8g'nd ($Q\simeq -7.5$ MeV) reaction at 28.0 MeV when θ_1 is fixed at 50°. The solid lines show the energies of the alpha-particles corresponding to the sequential decay process.

the quasi-free scattering analysis is performed. Three angular correlation distributions of the C^{12} $(\alpha, 2\alpha)$ Be^8 reaction, ($\theta_1=25°$, 35°, and 50°) are given in Figs. 42~44. in the $E_1-\theta_2$ plane. The sequential decay from some excited states of C^{12} are found as indicated in the figure, but does not affect so much our analysis on the quasi-free scattering.

For the Be^9 $(\alpha, 2\alpha)$ He^5 reaction, the same analysis as for B^{10} and C^{12} shows no apparent evidence of the sequential decay process.

4.3. Alpha-Clustering Correlation in Light Nuclei

4.3.1. *General*

Among many kinds of nucleon-clustering correlation, alpha-clustering has been most frequently treated in the theory and the experiment. In the early alpha-particle model of light nuclei, the alpha-particle in the nucleus was thought to maintain perfectly the nature of a free alpha-particle. At present, such a concept is proved to be quite wrong.[29] An alpha-particle which is stable in the nuclear field but disintegrates in the free space is considered as an alpha-cluster. Such an alpha-cluster has been treated from various points of view. One of the treatments is as follows: on the bases of the "resonating group theory" of Wheeler,[30] the nucleus is thought as a composite system of clusters, the nature of the nucleus is discussed from the interaction between the clusters. This is generally called the "cluster model".[3~5] Another treatment[31] starts from the single-particle wave function of the shell model and the reduced width of the various kinds of composite particles and other properties of the nucleus are discussed by means of the coupling of the nucleons and the configuration mixing of the states.

The most hopeful and topical treatment, belonging to the first method described above, is to construct the wave function of the cluster and the interaction between the clusters on the base of the realistic two-body nuclear force. Such a treatment has been applied to Be^9 and suceeded in the explanation of the properties of this nucleus.[5]

The reduced width only is not enough to inform the properties of the alpha-cluster correlation in the nucleus. Also the mean distance between two clusters is essential.[5,32]

The quantity P in equation (16) which has been decided by the analysis of the experimental angular correlation distribution, can be considered to give the probability of finding the alpha cluster in the nucleus $P\alpha$ after taking into account the normalization. The quantity α is considered to be related to the distance between the alpha-cluster and the core in the nucleus ($\beta=\alpha^2/2$). When a reasonable approximation is adopted about the motion of the particles in the nucleus, parameter β' which is related to the distance between the alpha-clusters in the nucleus can be obtained from β. The value of β' can be compared with the parameter γ of He^4. The value of γ obtained from the electron scattering experiment is $\gamma=0.433\ \mathrm{fm}^{-2}$.[1]

The ratio $x=\gamma/\beta'$ is often used to see the degree of isolation of alpha-clusters. The smaller the value of x is, the more the alpha-clusters are spacially isolated. When $x=0$, the alpha-clusters do not overlap. As x increases from zero to a value comparable with unity, the distance between the clusters becomes comparable with their internal sizes and when $x=1$, the cluster model wave function coincides the shell model wave function, with LS coupling.[3]

Table 1. The value of α and P, which are the parameters of the spread and the amplitude of the momentum distribution, respectively, obtained from the analysis of the experimental angular correlation distribution. And the value of β, P_α, β', and x, which are the parameters of the spacial spread between an alpha-cluster and the core, the probability of finding alpha-clusters in nucleus, the spacial spread between the two alpha-clusters in the nucleus and the degree of the spacial localization of the alpha-cluster in the nucleus, respectively, derived from the experimental value as described in the text.

Nucleus	L	α (fm^{-1})	P ($fm^3 \cdot st^{-1}$)	β (fm^{-2})	P_α	β' (fm^{-2})	x
Be^9	0	0.40	0.88	0.26	1.81	0.21	0.49
B^{10}	2	0.57	0.27	0.45		0.31	0.70
C^{12}	0	0.80	3.64×10^{-2}	0.67	0.34	0.38	0.87
O^{16}	0	0.34	0.51	0.10	0.26	0.07	0.16

The value of P obtained from our experiment, the value of P_α derived from P, the value of α obtained from our experiment and the value of β' derived from α by assuming a simple geometrical structure of the nucleus are given in Table I.

4. 3. 2. Be^9 *Nucleus*

Assuming that the Be^9 nucleus is constructed with two alpha-particles and one neutron and considering only the kinematical condition among them, $\beta'=0.21\ fm^{-2}$ is derived. Then, $x=0.49$ is obtained. This means that the alpha clusters in Be^9 are fairly well localized. The value of P_α, derived from the value of P, is $P_\alpha=1.81$. This value is very close to the effective number of alpha-cluster in Be^9 ($N_{eff}=2$). These facts show that the alpha-clustering correlation is very strong in Be^9.

For the Be^9 nucleus, some theoretical treatments on the base of the cluster model have been done. In the alpha-particle model of Kuntz,[4] the motion between two alpha particles in Be^8 core has been assumed to be the same as that in the Be^8 nucleus and only the motion between the extra neutron and the Be^8 core has been varied. This model has succeeded to give the excitation energy of the lower states of the Be^9 nucleus but has given three times larger value of quadrupole moment than the experimental value. This discrepancy may be due to the assumption that the motion between alpha particles in Be^9 is the same as that in Be^8 nucleus.

The equilibrium distance between two alpha particles was fixed at 4.60 fm, which corresponds to $\beta'=0.07\ fm^{-2}$. This value is much smaller than our experimental result. In the models of Wildermuth et. al.[34] and Hiura and Shimodaya,[5] the motion between two alpha particles in Be^9 is also varied. In the former model, the all nucleons which constrnct each cluster are treated in the same harmonic-oscillator potential. The properties of the lower states of Be^9 are mostly well explained when $\beta'=0.242\ f^{-2}$. In the latter model, the motion between the clusters is treated by the phenomenological interaction based on the realistic two-body nuclear force. The best agreement is obtained with the properties of the lower states and the value of the quadrupole moment when $\beta'=0.21\ fm^{-2}$.

Comparing with our experimental results, the last model gives best account of

the value of β'. Hiura and Shimodaya, also, have calculated one of our experimental angular correlation distribution on the bases of their alpha particle model of Be^9 and have got fairly good results about the amplitude and the shape of the momentum distribution.

4. 3. 3. B^{10} *Nucleus*

Assuming that the B^{10} nucleus is constructed with two alpha particles and one deuteron and considering only the kinematical condition among them, $\beta'=0.314\ f^{-2}$ is derived. Then $x=0.7$ is obtained.

With some uncertainty in the analysis of the angular correlation distribution, it can be said that the values of β' and P_α are not so far apart from the accurate value. These values indicate that the alpha clustering correlation is somewhat weaker in the B^{10} nucleus in comparison with the Be^9 nucleus.

From the calculated value of the reduced width of alpha-particles on the bases of the intermediate coupling shell model,[35] it has been predicted that the fractional parentage coefficient for the coupling between the alpha-particle and the ground state of Li^6 in the ground state of B^{10} nucleus is very small, in comparison with that for the coupling between the alpha-particle and the ground state of the core in Be^9, C^{12}, and O^{16}. However, the value of P derived from our experimental result is not so small.

4. 3. 4. C^{12} *Nucleus*

Assuming that the C^{12} nucleus is constructed with three alpha particles and that these three particles form the regular triangle and considering only the kinematical condition among them, $\beta'=0.377\ f^{-2}$ is derived. Then $x=0.87$ is obtained. The value of P_α is derived to be 0.344.

These facts may indicate that the alpha-clustering correlation is fairly weak in the C^{12} nucleus.

The value of x is very close to the prediction from the nucleon cluster model of Smirnov et al.[36] They have obtained, 0.8~0.9 for x, by comparing their model with the experimental E2 transition probability in C^{12}. It is indicated that the alpha-clusters in C^{12} are not so isolated that the anti-symmetrization among the nucleons in the alpha-clusters becomes important.

4. 3. 5. O^{16} *Nucleus*

Although our experimental result is not sufficient to discuss quantitatively, it is worth while to perform the similar discussion as Be^9, B^{10} and C^{12} in order to see the characteristics crudely. Assume that the O^{16} nucleus is constructed with four alpha-particles and that these four particles form the regular tetrahedron. Considering only the kinematical condition among them, $\beta'=0.0684\ f^{-2}$ is derived. Then the value of x becomes 0.16. The value of P_α is derived to be 0.262.

The value of P_α depends strongly on the value of α, so that it is better to compare the value of P of O^{16} with that of Be^9 and C^{12}. Then, it is found that P of O^{16} is more than one order larger than that of C^{12}.

These facts indicate that the alpha-clustering correlation is stronger in the O^{16} nucleus than that in the C^{12} nucleus, and that the alpha-clustering correlation is an important nature of O^{16}.

The value of x has been predicted from the nucleon cluster model to be 0.7 using the experimental E3 transition probability.[36] The tendency that x is rather small in O^{16} than in C^{12}, is consistent with our result. On the otherhand the reduced width of the alpha-particles which are coupled with the ground state of

the core nucleus has been predicted from the intermediate coupling shell model,[35] and has larger value in C^{12} than in O^{16}. This is not in accordance with our result. To clarify this problem, more experimental works must be done.

5. Concluding Remarks

The evidence for the quasi-free scattering process as a main part of the (α, 2α) and the (p, $p\alpha$) reaction is obtained. The Be^9 (α, 2α) $He^5_{g'nd}$ reaction is fairly well explained by the simple calculation based on the plane wave impulse approximation. Furthermore, in the reactions on B^{10}, C^{12} and O^{16}, the various shape of the angular correlation distributions are well explained qualitatively by our simple calculation. These facts show that our simple calculation is useful as the first approximation. The good fits in the case of Be^9 may be due to the small reaction Q value, the strong alpha-clustering correlation and the hardness of the alpha-particle (large binding energy and rather weak interaction with the other particle). In the reaction on the other nuclei, the increase of the reaction Q value may have more severe effect, that is, the incoming and outgoing waves is more distorted and the alpha-particle in the nucleus is more disturbed and more disintegrated in comparison with the free alpha particle. To ascertain the problem, more theoretical investigations (using the distorted waves for the incoming and outgoing particles and the interaction between the disturbed and disintegrating alpha-particle and the free alpha-particle) and more experimental investigations (using various energy and various kinds of incident particles) are needed.

Informations on the alpha-clustering correlation are also obtained. In the Be^9 nucleus, the correlation is strong and the alpha-particle model is supported. The results on C^{12} and O^{16} can be interpreted that the alpha-clustering correlation is rather strong in O^{16} than in C^{12}. This is a very interesting feature to investigate the effect of the many nucleon correlation in the nuclear many-body system. More experimental and theoretical works are needed especially on the O^{16} nucleus.

The sequential decay process is found about some excited states of the intermediate state nucleus (B^{10} and C^{12}). To separate the direct-interaction process from the sequential process more clearly, the azimuthal angular correlation experiment is thought to be useful. In experiment the distribution from the direct interaction mechanism shall be sharpened while that from the sequential decay process broadened.

In conclusion, the measurement of the direct knock-out reactions, such as (α, 2α) and (p, $p\alpha$) reaction in medium-energy region, seems to serve as a good tool to get informations on the properties of the alpha and the other clustering correlations in the nucleus. More experimental and theoretical works on their reaction mechanism and the nucleon clustering (especially alpha-clustering) correlations in the nucleus are to be hoped.

Acknowledgements

The author wishes to express his cordial thanks to Professors J. Muto, T. Yanabu and Y. Uemura for their advices and encouragements. His sincere thanks are due to Professors T. Yanabu and J. Muto and Dr. S. Yamashita for read and criticized the manuscript. He is much indebted to Professor T. Yanabu, Dr. S. Yamashita, Mr. K. Ogino, Mr. K. Hosono, Mr. S. Matsuki, and Mr. T. Tanabe for

their valuable suggestions, stimulating discussion and helpful co-operation to this work. His thanks are also due to the members of the Cyclotron Laboratory of Kyoto University for their helps and hospitalities and also to the members of the Institute of Nuclear Study of Tokyo University for use of the cyclotrons and the other facilities. He wish to thank Professor H. Tanaka, Dr. J. Hiure and Dr. I. Shimodaya in Hokkaido University and Prof. T. Honda in Tohoku University, and Dr. Y. Kudo in Osaka City University, and Prof. Y. Sakamoto in Kyoto University for their valuable discussions of this experimental results. The author would like to thank Professors. K. Nishimura and I. Kumabe and other members in his laboratory for their valuable discussions and hospitalities throughout the course of this work.

REFERENCES

1) R. Hofstadter: Rev. mod. Phys., **28** (1956) 214.
2) D. H. Wilkinson: Proceedings of the Rutherford Jubilee International Conference, Manchester, 1961, edited by J. B. Birks (Academic Press Inc., New York, 1961), p. 339.
3) R. K. Sheline and K. Wildermuth: Nucl. Phys., **21** (1960) 196. V. G. Neudachin, Yu. F. Smirnov and N. P. Yudin: Soviet Physics JETP., **37** (1959) 1781.
4) G. C. Phillips and T. A. Tombrello: Nucl. Phys., **19** (1960) 555. P. D. Kuntz: Ann. of Phys., **11** (1960) 275.
5) J. Hiura and I. Shimodaya: Prog. theor. Phys., **30** (1963) 585.
6) P. E. Brown, J. S. Blair, D. Bodansky, N. Cue and C. D. Kavaloski: Phys. Rev., **138** (1965) B1394. M. N. Huberman, M. Kamegai and G. C. Morrison: *ibid.*, **129** (1963) 791. D. S. Gemmell, J. R. Erskine, and J. P. Schiffer: *ibid.*, **136** (1964) B1325. V. K. Lukyanov and I. Ž. Petkov: Nucl. Phys., **49** (1963) 529.
7) S. S. Vasiliev, V. V. Komarov, G. V. Koshelyaev and A. M. Popova: Soviet Physics-JETP., **37** (1960) 1034. A. Sammon and P. Cüer: J. Phys. radium, **19** (1958) 13. C. Ruhla, M. Riou, J. P. Garron, J. P. Jacmart and L. Massonnet: Phys. Lett., **2** (1962) 44.
8) M. Lefort, J. P. Cohen, H. Dubost and X. Tarrago: Phys. Rev., **139** (1965) B1500. N. L. Den: Phys. Lett., **18** (1965) 158.
9) D. H. Wilkinson: Phil. Mag., **4** (1959) 215; B. D. Jones, B. Sanjeevaiah, J. Zakrzewski, P. G. Bizzeti, J. P. Lagnawx and M. René: Nuovo Ciment. **19** (1961) 1077; R. I. Jibuti, T. I. Kopaleishvili and V. I. Mamasakhlisov: Nucl. Phys., **52** (1964) 345. A. T. Bareslo-neev: Ž. eksp. teor. Fiz., **42** (1962) 713; R. I. Jibuti and T. I. Kopaleishvili: Nucl. Phys., **55** (1964) 337.
10) D. A. Bromley, Kuelmer and Almqvist: Phys. Rev. Ltters, **4** (1960) 363.
11) I. Shimodaya, R. Tamagaki and H. Tanaka: Prog. Theor. Phys., **27** (1962) 793; R. Tamagaki and H. Tanaka: *ibid*, **34** (1965) 191. S. Okai and S. C. Park: Phys. Rev., **145** (1966) 787.
12) A. N. James and H. G. Pugh: Nucl. Phys., **42** (1963) 441; C. Ruhla, M. Riou, M. Gusakow, J. C. Jacmart, M. Lin and L. Valentin: Phys. Lett., **6** (1964) 318.
13) T. J. Gooding and G. Igo: Phys. Rev. Letters, **7** (1961) 28; G. Igo, L. F. Hansen and T. J. Gooding: Phys. Rev., **131** (1963) 337.
14) P. Darriulat, G. Igo, H. G. Pugh and H. G. Holmgren: Phys. Rev., **137** (1965) B315.
15) T. Yanabu, S. Yamashita, K. Takimoto and K. Ogino: J. Phys. Soc. Japan, **20** (1965) 1303.
16) T. Yanabu, S. Yamashita, R. Ishiwari, K. Takimoto, K. Ogino, Y. Okuma, K. Hosono, S. Matsuki, T. Tanabe and S. Okumura (to be published).
17) T. Yanabu, S. Yamashita, R. Ishiwari, S. Kakigi, D. C. Nguyen, K. Takimoto, K. Ogino, K. Hosono, S. Matsuki and T. Tanabe (to be published).
18) T. Yanabu, S. Yamashita, K. Takimoto, K. Ogino, K. Hosono, S. Matsuki and T. Tanabe (to be published).

19) T. Yanabu, S. Yamashita, K. Takimoto, K. Ogino, K. Hosono, S. Matsuki and T. Tanabe (to be published).
20) T. Yanabu, S. Yamashita, S. Kakigi, D. C. Nguyen, K. Takimoto, K. Yamada and K. Ogino: J. Phys. Soc. Japan, **19** (1964) 1818.
21) K. L. Lim and I. E. MaCarthy: Phys. Rev., **133** (1964) B1006. T. Berggren and G. Jacob: Nucl. Phys., **47** (1963) 481.
22) H. Tyrén, S. Kullander, O. Sundberg, R. Ramachandran and P. Isacsson: Nucl. Phys, **79** (1966) 321.
23) G. F. Chew: Phys. Rev., **80** (1950) 196.
24) Y. Nishida: Nucl. Phys., 82 (1966) 385.
25) J. Hiura and I. Shimodaya: private communication.
26) M. Riou: Rev. mod. Phys., **37** (1965) 375.
27) T. Yanabu, S. Yamashita, T. Nakamura, H. Ogata, K. Takamatsu, A. Masaike, S. Kakigi, D. C. Nguyen, and K, Takimoto: Genshikaku Kenkyu (Circular in Japanese) vol. 8, p. 233.
28) G. C. Phillips, T. A. Griffy and L. C. Biedenharn: Nucl. Phys., **21** (1960) 327; E. H. Beckner, C. M. Jones and G. C. Phillips: Phys. Rev. **123** (1961) 255; P. F. Donovan, J. V. Kane, Č. Zupančič, C. P. Baker and J. F. Mollenauer: Phys. Rev., **135** (1965) B61. Č. Zupančič: Rev. mod. Phys., **37** (1965) 330. G. C. Phillips: *ibid.*, **37** (1965) 409.
29) J. M. Blatt and V. F. Weisskopf: "Theoretical Nuclear Physics" (John Wiley & Sons, New York, 1954) p. 292.
30) J. A. Wheeler: Phys. Rev., **52** (1937) 1107.
31) V. V. Balashov and I. Rotter: Nucl. Phys., **61** (1965) 138.
32) Yu. F. Smirnov and D. Chlebowska: Nucl. Phys., **26** (1961) 306.
33) J. Hiura and I. Shimodaya: Prog. Theor. Phys., **34** (1965) 861 ; *ibid.*, **36** (1966) 977.
34) Y. C. Tang, F. C. Khanna, P. C. Herndon and K. Wildermnth: Nucl. Phys., **35** (1962) 421.
35) V. V. Balashov, A. N. Boyarkina and I. Potter: Nncl. Phys., **59** (1964) 417.
36) Yu. A. Kudeyarov, Z. Matthies, V. G. Neudachin and Yu. F. Smirnov: Nucl. Phys., **65** (1965) 529.